

APPROVAL SHEET

Title of Thesis: Comparison of the Chirped Return-to-Zero and
Dispersion Managed Soliton Modulation Formats
in Wavelength Division Multiplexed Systems

Name of Candidate: Ruo-Mei Mu
Doctor of Philosophy, 2001

Dissertation and Abstract Approved: _____
Professor Curtis R. Menyuk
Computer Science and Electrical Engineering

Date Approved: _____

Curriculum Vitæ

Name: Ruo-Mei Mu

Permanent Address: P. O. Box 22,
Beijing University of Posts and Telecommunications,
Beijing, P. R. China, 100088.

Degree and date to be conferred: Ph.D., August, 2001.

Date of Birth: September 15, 1969.

Place of Birth: Baotou, Neimeng, P. R. China.

Secondary education: No.1 Baotou Steel Incorporation Middle School
Baotou, Neimeng, P. R. China,
July, 1987.

Collegiate institutions attended: 1987–1991, Beijing University of Posts and
Telecommunications, B.S., Jul. 1991,
1991–1996, Beijing University of Posts and
Telecommunications, Ph.D., Oct. 1996,
1996–2001, University of Maryland
Baltimore County, Ph.D., Aug. 2001.

Major: Photonics (Electrical Engineering).

Professional position: Research Assistant
Univer. of Maryland, Balti. Co.
TRC 202B, 1000 Hilltop Circle
Baltimore, MD 21250
Senior Member of Technical Staff
TyCom Inc.
250 Industrial Way–West
Eatontown, NJ 07724-2206.

Professional publications in archival journals:

1. R.-M. Mu, V. S. Grigoryan, C. R. Menyuk, E. A. Golovchenko, and A. N. Pilipetskii, "Timing-jitter Reduction in a Dispersion-Managed Soliton System," *Optics Lett.* **23**, 930–932 (1998).
2. R.-M. Mu, V. S. Grigoryan, C. R. Menyuk, G. M. Carter, and J. M. Jacob, "Comparison of Theory and Experiment for Dispersion-Managed Solitons in a Recirculating Fiber Loop," *IEEE J. Select. Topics Quantum Electron.* **6**, 248–257 (2000)
3. R.-M. Mu and C. R. Menyuk, "Symmetric Slope Compensation in a Long Haul WDM System Using the CRZ Format," *IEEE Photon. Technol. Lett.* (*to be published.*)
4. R.-M. Mu, T. Yu, V. S. Grigoryan, and C. R. Menyuk, "Dynamics of Chirped Return-to-Zero Format," (*submitted to J. Lightwave Technol. for publication.*)
5. R.-M. Mu and C. R. Menyuk, "Convergence of the Chirped Return-to-Zero and Dispersion Managed Soliton Modulation Formats in WDM Systems," (*submitted to J. Lightwave Technol. for publication.*)
6. T. Yu, R.-M. Mu, V. S. Grigoryan, and C. R. Menyuk, "Energy Enhancement of Dispersion-Managed Solitons in Optical Fiber Transmission Systems with Lumped Amplifiers," *IEEE Photon. Tech. Lett.* **10**, 75–77 (1999).
7. G. M. Carter, R.-M. Mu, V. S. Grigoryan, C. R. Menyuk, P. Sinha, T. F. Carruthers, M. L. Dennis, and I. N. Duling III, "Transmission of Dispersion-Managed Solitons at 20 Gbit/s over 20,000 km," *Electron. Lett.* **35**, 233–234 (1999).
8. V. S. Grigoryan, C. R. Menyuk, and R.-M. Mu, "Calculation of Timing and Amplitude Jitter in Dispersion-Managed Optical Fiber Communications Using Linearization," *J. Lightwave Technol.*, **17**, 1347–1356 (1999).
9. V. S. Grigoryan, R.-M. Mu, G. M. Carter, and C. R. Menyuk, "Experimental Demonstration of Long-Distance Dispersion-Managed Soliton Propagation at Zero Average Dispersion," *IEEE Photon. Tech. Lett.* **12**, 45–46 (2000).

10. X. Y. Tang, R.-M. Mu, and P. D. Ye, "Effect of Filters on Soliton Collisions in WDM Systems with Lumped Amplifiers and Periodically Varying Dispersion," *Opt. and Quantum Electron.* **26**, 969–976 (1994).

Professional publication in book chapter:

1. C. R. Menyuk, G. M. Carter, W. L. Kath, and R.-M. Mu, "Dispersion Managed Solitons & Chirped Return to Zero: What is the Difference?" (will appear in *Optical Fiber Telecommunications IV*, edited by T. Li and I. P. Kaminow, to be published by Academic Press.)

Professional contributions in conferences:

1. R.-M. Mu, V. S. Grigoryan, and C. R. Menyuk, G. M. Carter, and J. M. Jacob, "The Performance of a 10 Gbits/s Filtered Dispersion-Managed Soliton System with Lumped Amplifiers," Optical Fiber Communication Conference (OFC'99), San Diego, CA (Feb. 21–26, 1999), paper WC2.
2. G. M. Carter, R.-M. Mu, V. S. Grigoryan, P. Sinha, C. R. Menyuk, "20 Gb/s Transmission of Dispersion-Managed Solitons over 20,000 km," Optical Fiber Communication Conference (OFC'99), San Diego, CA (Feb. 21–26, 1999), paper WC1.
3. R.-M. Mu, V. S. Grigoryan, C. R. Menyuk, G. M. Carter, J. M. Jacob, and P. K. A. Wai, "Filtered Dispersion-Managed Solitons in Anomalous and Normal Dispersion Regimes," Optical Society of America Annual Meeting (OSA'98), Baltimore, MD (Oct. 4–9, 1998), paper ThC2.
4. V. S. Grigoryan, C. R. Menyuk, G. M. Carter, and R.-M. Mu, "Tolerance of Dispersion-Managed Soliton Transmission to the Shape of the Input Pulses," Optical Society of America Annual Meeting (OSA'98), Baltimore, MD (Oct. 4–9, 1998), paper ThC3.
5. R.-M. Mu, T. Yu, V. S. Grigoryan, E. A. Golovchenko, A. N. Pilipetskii, and C. R. Menyuk, "Optimizing the Arrangement of Optical Amplifiers in a Dispersion-Managed Soliton System," Optical Fiber Communication Conference (OFC'98), San Jose, CA (Feb. 22–27, 1998), paper ThC5.
6. V. S. Grigoryan, C. R. Menyuk, and R.-M. Mu, "Timing Jitter in Dispersion-Managed Soliton Communications," Optical Fiber Communication Conference (OFC'98) San Jose, CA (Feb. 22–27, 1998), paper ThC3.
7. R.-M. Mu, V. S. Grigoryan, E. A. Golovchenko, A. N. Pilipetskii, T. Yu, and C. R. Menyuk, "Timing Jitter Reduction in a Dispersion-Managed Soliton System," Optical Society of America Annual Meeting (OSA'98), Long Beach, CA (Oct. 12–17, 1997), paper FC2.
8. T. Yu, R.-M. Mu, E. A. Golovchenko, A. N. Pilipetskii, V. S. Grigoryan, and C.R. Menyuk, "Energy Enhancement of Dispersion-Managed Solitons in Optical Fiber Transmission Systems With Lumped Amplifiers," Optical Society of Ame-

- rica Annual Meeting (OSA'98), Long Beach, CA (Oct. 12–17, 1997), paper ThI4.
9. V. S. Grigoryan, R.-M. Mu, G. M. Carter, and C. R. Menyuk, “Experimental Demonstration of Long-Distance Dispersion-Managed Soliton Propagation at Zero Average Dispersion,” Conference on Lasers and Electro-Optics (CLEO'99), Baltimore, MD (May 23–28, 1999), paper CMH4.
 10. R.-M. Mu, V. S. Grigoryan, G. M. Carter, and C. R. Menyuk, “Propagating a 4×10 Gbit/s Wavelength-Divisioned Multiplexed System with Channel Spacing of 0.5 nm Over 10,000 km Using Quasi Dispersion-Managed Soliton and Inline MUX/DEMUX Modules,” Optical Society of America Annual Meeting (OSA'99), Santa Clara, CA (Sept. 26–30, 1999), paper WV3.
 11. R.-M. Mu, T. Yu, V. S. Grigoryan, and C. R. Menyuk, “Convergence of the CRZ and DMS Formats in WDM Systems Using Dispersion Management,” Optical Fiber Communication Conference (OFC'2000) Baltimore, MD (Mar. 5–10, 2000), paper FC1.
 12. V. S. Grigoryan, C. R. Menyuk, and R.-M. Mu, “Pulse Jitter in Fiber Communications,” 1997 AFOSR Workshop on Nonlinear Optics, Tucson, AZ (Sept. 24–26, 1997).
 13. C. R. Menyuk, T. Yu, R.-M. Mu, and D. Wang, “New Approaches to Modeling High Data Rate Optical Fiber Transmission Systems,” Optoelectronics Industry Development Association 1998 Annual Membership Forum, Washington, DC (Oct. 1–2, 1998).
 14. V. S. Grigoryan, R.-M. Mu, D. Wang, T. Yu, and C. R. Menyuk, “New Approaches to Modeling Optical Fiber Transmission Systems,” The 1999 IMACS International Conference on Nonlinear Evolution Equations and Wave Phenomena: Computation and Theory, Athens, GA (April 12–16, 1999).
 15. C. R. Menyuk, R.-M. Mu, D. Wang, T. Yu, and V. S. Grigoryan, “New Approaches to Modeling Optical Fiber Transmission Systems,” IMA Workshop: Analysis and Modeling of Optical Devices, Minneapolis, MN (Sept. 9–10, 1999).
 16. C. R. Menyuk, R.-M. Mu, D. Wang, T. Yu, and V. S. Grigoryan, “New Approaches to Modeling Optical Fiber Transmission Systems,” 1999 AFOSR Workshop on Nonlinear Optics, Tucson, AZ (Sept. 16–18, 1999).

- 17 C. R. Menyuk, V. S. Grigoryan, R.-M. Mu, D. Wang, and T. Yu “Modeling High-Data-Rate Optical Fiber Communication Systems,” short course at Optical Fiber Communication Conference (OFC’99), San Diego, CA, (Feb. 21–26, 1999)
18. C. R. Menyuk and R.-M. Mu, “Dispersion-Managed Solitons & Chirped Return-to-Zero: What is the Difference?” Optoelectronics and Communications Conference, Makuhari Messe, Chiba, Japan (July 10–14, 2000), paper WS1-8.
19. R.-M. Mu and C. R. Menyuk, “Symmetric Slope Compensation in a Long Haul WDM System Using the CRZ Format,” (*submitted to Optical Society of America Annual Meeting (OSA ’01)*).
20. C. R. Menyuk and R.-M. Mu, “Dispersion-Managed Solitons & Chirped Return to Zero: What is the Difference?” (*submitted to Nineteenth Symposium on Energy Engineering Sciences.*)
21. R.-M. Mu, and P. D. Ye, “Switching Character of Solitons in Active Birefringent Fiber,” International Conference on Communications Technology (ICCT’96), Beijing, China, (May 5–7, 1996), paper pp 104–108.
22. R.-M. Mu, and P. D. Ye, “Limitation of Soliton Transmission System Employing Soliton Control Technology under Optimal System Design,” International Conference on Information Infrastructure (ICII’96), Beijing, China, (April 25–28, 1996).
23. R.-M. Mu, and P. D. Ye, “Optimal Design Theory for Ultrahigh Soliton Transmission System with Control Technology,” International Conference on Applications of Photonic Technology (ICAPT’96), Montreal, Canada, (July 29–August 1, 1996).
24. R.-M. Mu, and P. D. Ye, “Numerical Study of Generating Transform-Limited Soliton Trains by Gaussian Pulses through Nonlinear Fiber,” 1995 Sino-Japanese Joint Meeting on Optical Fiber Science and Electromagnetic Theory (OFSET’95), Tianjing, China, (September 20–22, 1995).
25. R.-M. Mu, and P. D. Ye, “Analysis on Energy Fluctuation in High Speed Optical Soliton Transmission Systems over Long Distance with Soliton Controlling”, Conference on Lasers and Electro-Optics/Pacific Rim (CLEO/Pacific Rim ’95), Chiba, Japan, (July 10–14, 1995), paper TuO3.

26. R.-M. Mu, and P. D. Ye, "Filter in the Optical Soliton Transmission System," International Conference on Communications Technology (ICCT'94), Shanghai, China, (June 8–10, 1994), paper pp 202–205.
27. R.-M. Mu, X. Y. Tang, and P. D. Ye, "Bit Error Rate of Optical Soliton Communication Systems with Lumped Amplifiers and Guiding-Frequency Filters", 1993 IEEE Region 10 Conference on Energy, Communication, Computer and Controls (IEEE TENCON '93), Beijing, China, (Oct 19–21, 1993), pp. 505–508.
28. X. Y. Tang, R.-M. Mu, and P. D. Ye, "Analysis of Soliton Collisions in Wavelength Division Multiplex Systems with Lumped Amplifiers and Frequency-Guiding Filters", The international Society for Optical Engineering (SPIE)'s International Symposium for Multigigabit Fiber Communication Systems (SPIE San Diego '93), San Diego, CA, (July 11–16, 1993), SPIE Proceedings Vol. 2024, pp. 81–86.

Abstract

Title of Dissertation: Comparison of the Chirped Return-to-Zero and Dispersion Managed Soliton Modulation Formats in Wavelength Division Multiplexed Systems

Ruo-Mei Mu, Doctor of Philosophy, 2001

Dissertation directed by: Professor Curtis R. Menyuk
Computer Science and Electrical Engineering

I numerically simulated long-distance, high-bit-rate, wavelength-division-multiplexed transmission in dispersion-managed systems. I investigated chirped return-to-zero (CRZ) and dispersion managed soliton (DMS) formats that have been employed in experimental demonstration systems—including the Tyco-CRZ system [1], [2], the CNET-DMS system [3]–[5], and the KDD-RZ system [6]–[9]—as well as our own system at University of Maryland Baltimore County (UMBC) [10]–[15]. Consistent with earlier experiments, I find that the chirped return-to-zero format has significant advantages over the periodically stationary dispersion-managed soliton format in wavelength-division-multiplexed systems. Hence, the dispersion-managed soliton and the chirped return-to-zero pulse formats used in practice have converged toward a quasilinear evolution that is not periodically stationary. I elucidate the physical reasons for these advantages. I will discuss in detail the dynamics of the chirped

return-to-zero systems, carefully distinguishing noise effects, single-channel nonlinear effects, and multi-channel nonlinear effects. In this way, I provide a physical basis for understanding chirped return-to-zero systems that should prove useful for future system design. In particular, I find that the pulse evolution is dominated by linear dispersion and that the spread in the eye diagram is dominated by signal-spontaneous beat noise, just like in linear systems, although nonlinearity plays an important role and must be carefully mitigated.

**Comparison of the Chirped Return-to-Zero and
Dispersion Managed Soliton Modulation
Formats in Wavelength Division
Multiplexed Systems**

by

Ruo-Mei Mu

Dissertation submitted to the Faculty of the Graduate School
of the University of Maryland in partial fulfillment
of the requirements for the degree of
Doctor of Philosophy
2001

© Copyright by Ruo-Mei Mu, 2001

Dedication

To my family, my parents, and my sister

Acknowledgements

I wish I could express my greatest gratitude to my advisor, Professor Curtis Menyuk: for his endless guidance and professional perfection as well as for his incessant encouragement and extreme patience throughout the course of my dissertation research.

I would like to thank sincerely to Professor Gary Carter, Professor Fow-Sen Choa, Professor Li Yan, Dr. Heider Ereifej, and Dr. Alexei Pilipetskii, for their time and effort in going through the dissertation.

My special thanks go to Dr. Jeff Livas, Dr. Michael Frankel, and Dr. Shuxian Song at Ciena Corporation. The unique experience of working with them has enhanced my career vision.

I also want to thank all my colleagues and friends who helped me through this long journey. I am grateful for all the knowledge that I have learned from them: Dr. Ping-Kong (Alex) Wai, Dr. Ekaterina Golovchenko, Dr. John Jacob, Dr. Pranay Sinha, Dr. Vladimir Grigoryan, Dr. Edem Ibragimov, Dr. Tao Yu, Dr. Ding Wang, Dr. John Zweck, Dr. Brian Marks, Ivan, Ronald, Oleg and Aurenice. Sincere thanks go to my friends, Yu and Zheng, ShanShan and Rouyong, Kejian and Liang, the best friends I ever had.

At last, I would like to dedicate all my accomplishments to my family, my parents, and my sister who have always been there for me.

TABLE OF CONTENTS

List of Tables	vi
List of Figures	vii
1 Introduction	1
2 Mathematical models	6
2.1 Modified NLS equations	6
2.2 Gain saturation model	7
2.3 Scale length	9
2.4 Evaluation of the system performance	10
3 Study of the timing jitter in a DMS system—validation of the ASE model	12
4 Comparison between theory and experiment for a single channel DMS system in a recirculating loop	17
4.1 System setup	18
4.2 Dynamics of Dispersion Managed Solitons	20
4.3 System Performance in the Presence of Amplified Spontaneous Emission Noise	23

5	Testing the feasibility of a 4×10 Gbit/s WDM system using a periodically stationery DMS format	28
5.1	Primary system design	30
5.2	Nonlinear pulses propagation	33
5.3	Evaluation of multi-channel performance	38
6	Convergence of the Tyco-CRZ, CNET-DMS, and KDD-RZ WDM systems	41
6.1	Introduction	41
6.2	Schematic configurations of the Tyco-CRZ, CNET-DMS, and KDD-RZ systems	44
6.3	Intra-channel system behavior	51
6.4	WDM studies	64
6.5	Conclusion	73
7	Conclusion	75
	Bibliography	78

List of Tables

6.1	The fiber parameters in three model WDM systems. (a) Tyco-CRZ system, (b) CNET-DMS system, and (c) KDD-RZ system.....	50
6.2	The fiber parameters in (a) Tyco-CRZ system, (b) CNET-DMS system, and (c) KDD-RZ system for a typical channel selected in the single channel studies.....	52
6.3	The residual average dispersion in the 8 WDM channels of the KDD-RZ system, where Ch. = channel.....	66

List of Figures

- 3.1 The timing jitter as a function of distance with amplifiers spaced 50 km. The curves (1) correspond to the timing jitter in a standard soliton system with uniform dispersion fiber. The dashed line is the analytical result from Gordon-Haus theory [16], while the solid line shows the result of the Monte Carlo simulations. Curve (2) corresponds to the timing jitter in a dispersion-managed soliton system. The circles show the result of the semi-analytical approach [17], while the solid line shows the result of the Monte Carlo simulations. Curve (3) shows the modified Gordon-Haus result [18] 14
- 3.2 The timing jitter as a function of distance with amplifiers spaced 100 km and put at the points of maximum pulse expansion in the dispersion map. The curves (1), (2), and (3) are as in Fig. 3.1. 16
- 4.1 The experimental setup for the 10 Gbit/s DMS transmission over 24,500 km [11]. Small circles along the loop show the tap points at which experimental data could be extracted. 19

4.2	The influence of different gain models on the stabilization of the DMS pulse propagation with $\overline{D} = 0.02$ ps/nm-km. (a) Without gain saturation, $G_0 = 31.6$ dB with $G_{a,0} = 5.0$ dB and $G_{b,0} = 11.6$ dB, and $P_{in} = 9$ dBm. (b) Without gain saturation, $G_0 = 31.5$ dB with $G_{a,0} = 5.0$ dB and $G_{b,0} = 11.5$ dB, and $P_{in} = 9$ dBm. (c) Without gain saturation, $G_0 = 31.6$ dB with $G_{a,0} = 5.0$ dB and $G_{b,0} = 11.6$ dB, and $P_{in} = 5$ dBm. (d) With gain saturation, $G_0 = 32.45$ dB and $P_{in} = 9$ dBm. (e) With gain saturation, $G_0 = 32.45$ dB and $P_{in} = 5$ dBm. In cases (d) and (e), $G_{a,0} = 5.4$ dB, and $G_{b,0} = 10.85$ dB.	21
4.3	The dynamics of the DMS signal at steady-state. I show the (a) duration, (b) peak power, and (c) the chirp of the pulse as functions of distance during one round trip in the loop. The squares show the experimentally measured pulse durations.	22
4.4	Timing jitter as a function of the transmission distance in a single channel experiment.	24
4.5	Amplitude margin along the transmission line at a bit rate of 10 Gbit/s. The upper curve shows the decision level of the marks, and the lower curve shows the decision level of the spaces. Squares and circles are the experimental data.	25
4.6	The experimental setup for the 20 Gbit/s DMS transmission [15]. The white circles represent the normal disperison fiber while the gray ones correspond to the anomalous fiber.	26
4.7	Amplitude margin along the transmission line at a bit rate of 20 Gbit/s. Solid lines are simulation results while squares and circles corresponding to the experimental data.	27

5.1	A 4×10 Gbit/s experimentally scaled WDM transmission system, where the dispersion slope compensator (DSC) includes a MUX/DEMUX pair with single mode fiber, dispersion compensating fiber and EDFAs...	31
5.2	The power margins as a function of path average dispersion \bar{D} at 1.551 μm .	32
5.3	Pulse propagation of a single channel using the transmission setup shown in Fig. 5.1	33
5.4	Pulse breathing inside one loop period at the steady state. The solid line represents the evolution of the pulse duration, and the dashed line represents the variation of the pulse chirp.	34
5.5	Evolution of the pulse RMS spectral intensity. The dashed line with filled squares represents the spectral evolution in a linear system	35
5.6	The growth of the pulse RMS duration in the frequency domain inside one loop period.	36
5.7	The evolution of the pulse time-bandwidth product along the transmission.	36
5.8	The received eye diagram for the single channel propagation.	37
5.9	The power margin in the single channel case.	37
5.10	The evolution of the signal spectrum. While (a) represents the input and (b) corresponds to the output.	38
5.11	The evolution of the spectrum, while (a) corresponds to the input and (b) shows the output after 10,000 km propagation.	39
5.12	The output eye diagrams of all the channels in the system.	39
5.13	Timing jitter as a function of distance in the system.	40
5.14	The Q -values as a function of distance in the system. The lower dashed line represents $Q = 6$ corresponding to a BER $\leq 10^{-9}$.	40

6.1	Schematic configuration of the three WDM model transmission systems: (a) Tyco-CRZ system, (b) CNET-DMS system, and (c) KDD-RZ system.	46
6.2	Evolution of the FWHM pulse duration at the end of each map period in the Tyco-CRZ system.	52
6.3	Evolution of the FWHM pulse duration at the end of each map period in the CNET-DMS system.	53
6.4	Evolution of the FWHM pulse duration at the end of each map period in the KDD-RZ system.	54
6.5	Dependence on the chirp C of (a) the final pulse compression and (b) the optimal residual average dispersion in Tyco-CRZ and CNET-DMS systems. The short-dashed lines with filled circles are the results predicted by modified linear theory, the solid lines with squares represent the result of full nonlinear model, while the long-dashed lines with triangles represent to the prediction from Gaussian theory. The left side corresponds to the results in Tyco-CRZ system while the right side represents the results in CNET-DMS system. I do not show Gaussian theory in the dependence of the chirp vs. the optimal residual average dispersion in the Tyco-CRZ system (the left lower figure) since there is no visible difference between the Gaussian theory and the modified linear theory.	56
6.6	Evolution of the pulse shape inside one map period in the mid-way in the Tyco-CRZ system.	57
6.7	Evolution of the pulse shape inside the last map period in the CNET-DMS system.	58

6.8	Evolution of the pulse shape inside the last map period in the KDD-RZ system	58
6.9	Eye diagrams in a single channel case in the Tyco-CRZ system, where (a) shows the case in which neither nonlinearity nor ASE noise is included in Eq. 2.1, (b) shows the case where we only neglect the ASE noise, (c) shows the case where I only neglect the nonlinearity in the simulations, and (d) shows the case where neither nonlinearity nor ASE is neglected.	59
6.10	Eye diagrams in a single channel case in the CNET-DMS system, where (a)–(d) are the same as in Fig. 6.9.	60
6.11	Eye diagrams in a single channel case in the KDD-RZ system, where (a)–(d) are the same as in Fig. 6.9.	60
6.12	Optical eyes before and after the transmission line in a single channel study in Tyco-CRZ system. I show (a) the input and (b)–(d) the output with (b) symmetric compensation, (c) pre-compensation, and (d) post-compensation.	61
6.13	The offset of the CRZ pulse pairs in the time and frequency domains, as well as the accumulated dispersion in the individual configurations: (a) symmetric compensation, (b) pre-compensation, and (c) post-compensation. The dashed line corresponds to the earlier pulse, and the solid line corresponds to the later pulse.	63
6.14	Evolution of the (a) input and (b) output spectral intensity in the Tyco-CRZ system.	67
6.15	Evolution of the (a) input and (b) output spectral intensity in the CNET-DMS system.	68

6.16 Evolution of the (a) input and (b) output spectral intensity in the KDD-RZ system.	69
6.17 Eye diagrams of three channels in the 7×10 Gbit/s Tyco-CRZ WDM system.	70
6.18 Eye diagrams of three channels in the 7×10 Gbit/s CNET-DMS WDM system.	71
6.19 Eye diagrams of three channels in the 8×10 Gbit/s KDD-RZ WDM system.	72

Chapter 1

Introduction

In just the last few years, the ever-increasing volume of digital information has turned wavelength-division-multiplexed (WDM) fiber communications systems into a billion-dollar mainstream business, and it has created what is perhaps the most rapid emergence of a new technology in the history of mankind. Especially, in the past couple of years, the true excitement is that this field has achieved a large degree of commercial applicability as central telephone administrations and network operators around the world recognize their need for tremendous network capacity growth due to the traffic demands for video and multimedia services. Fiber optical transport technology will play a significant role in helping to achieve the needed bandwidth. Consequently, the optical transmission systems and related technologies are being marketed by many major telecommunications equipment suppliers as well as a number of promising startup companies.

The time to bring research prototypes to the market has been shortened from several years to two years or even less [19]. It is generally recognized that the available bandwidth in optical fibers has been underutilized in traditional single-channel systems by about four orders of magnitude [20]. So it is natural to mine this band-

width resource by employing optical WDM tools. By now, WDM technology has made it possible to achieve high capacity systems of over 1 Tbit/s. The most exciting achievements were reported recently in the European Conference on Optical Communications. There were experimental demonstrations of systems with transmission rates of at least 5 Tbit/s. One was a 160 Gbit/s \times 40 WDM transmission system over 186 km from NEC [21]. The second was a 7 Tbit/s (176 \times 40 Gbit/s) bidirectional interleaved WDM transmission system with a 50 GHz channel spacing from Siemens AG [22]. The third was a 5.12 Tbit/s (128 \times 40 Gbit/s) system over 3 \times 100 km of TeraLightTM fiber from Alcatel [23]. In the long-haul transmission field, the most recent results include a 180 \times 10 Gbit/s WDM system over 7000 km with 0.4 (bits/s)/Hz spectral efficiency from TyCom [24], a 1 Tbit/s WDM transmission over 10,000 km with a channel spacing of 50 GHz from Fujitsu [25], a 1.1 Tbit/s (55 \times 20 Gbit/s) dense WDM soliton transmission system over 3,020 km from NEC [26], and a 211 \times 10 Gbit/s over 7,221 km with an amplifier spacing of 80 km that used Raman/EDFA hybrid in-line amplifiers [27]. One of the most daunting aspects of ultra-high capacity WDM experimental systems is the large amount of equipment that is required. Thus, increasing the bit rate per channel beyond tens of gigabits per second is a practical alternative to just expanding the number of optical wavelengths, which has the potential difficulty of requiring a tremendous amount of electrical power for the optical devices to be delivered through copper cables [28].

A fundamental limitation facing ultra-high-speed WDM transmission systems arises from the Scylla and Charybdis of fiber properties: chromatic dispersion and optical nonlinearity. Dispersion limits the bit rates achievable in a single optical channel according to the relation $B^2DL < 1.04 \times 10^5$ where B is the bit rate in gigabits/second [29]. The development of dispersion-shifted fiber (DSF) promised to

remove this limitation by redesigning the fiber index profile to generate a waveguide dispersion that cancels the material dispersion at the operating wavelength (typically 1550 nm). Unfortunately, this solution only removes dispersion. At the same time, it enhances the effect of the nonlinearity because fibers that operate near zero dispersion provide an ideal medium for phase-matched generation of new optical waves via four wave mixing. To reduce the four wave mixing, it requires a high local dispersion, while at the same time minimizing the pulse distortion requires a low cumulative dispersion. Modern systems use dispersion management in which sections of large positive dispersion alternate with sections of large negative dispersion. [30]–[33]. In contrast to DSF, the high local dispersion in the dispersion map destroys the phase matching that generates strong four wave mixing while at the same time keeping the path average dispersion low. Hence the transmission distance increases. In addition, the higher local dispersion can also be used to balance or manage the nonlinearity due to the inevitable increase of optical power in WDM systems. Furthermore, the invention of the dispersion compensating fiber (DCF) has made it possible to balance the accumulated fiber dispersion along the transmission line. Recently, new fibers have been developed that make it possible to reduce the total average dispersion slope among the WDM channels by providing a negative dispersion slope [5], [19]–[27].

A consequence of the universal use of dispersion management is that it might end the old debate, that has lasted nearly two decades, about the preferable data modulation format in high capacity systems—a soliton format or a non-soliton format such as non-return to zero (NRZ). As individual channel data rate and the number of WDM channels have continued to grow, both formats have evolved substantially. Solitons have evolved into dispersion managed solitons (DMS), and NRZ has evolved

into chirped return to zero (CRZ). These two types of systems resemble each other in many respects [34].

Adding the channels together in a WDM system inevitably increases the total optical signal power launched into the fiber link so that the fiber nonlinearity becomes significant during pulse propagation. Thus, the fiber nonlinearity is important in every WDM system no matter what format is used; however, the exact role of the fiber nonlinearity in each individual system remains unclear. Under these circumstances, it is worthwhile to carefully study the influence of the nonlinearity in current DMS and CRZ systems.

The basic goal of my dissertation is to theoretically compare the behaviors of both DMS and CRZ formats in WDM systems at 10 Gbit/s per channel so that one can carefully explore the physical impacts of the nonlinearity on these systems and find the optimal method to combat them in future WDM system design. Based on the successful simulation model that I have built [35], my investigation will be carried out by numerically evaluating the performance of the system including all the necessary physical phenomena. In addition to studying the performance of several influential experiments [1]–[9], I am also proposing a novel WDM configuration that can be built as a flexible experimental tool to investigate both the DMS and the CRZ formats. This system setup allows the users to compensate both the dispersion and gain variations as a function of frequency so that one can study both DMS and CRZ signals. The feasibility of transmitting quasi-DMS pulses at multiple wavelengths has been tested.

My investigation will be based on a variant of the nonlinear Schrödinger equation (NLS) that includes amplified spontaneous emission (ASE) noise and the actual system configuration. To determine an acceptable system performance, I will calculate

the timing jitter and the amplitude jitter individually. Using them, I will estimate the bit error rate (BER) and find the system parameters that are required to achieve a BER of less than 10^{-9} . The achievable power margin will be the key factor that determines the optimal system design.

The basic mathematical model guiding my numerical experiments is presented in Chap. 2. In Chap. 3, I describe the validation of my ASE model by studying the timing jitter in DMS systems. Then, I calibrate the performance of my simulator in more detail by comparing the simulation results against the measured results from the single channel DMS experiment built at Laboratory for Physical Sciences [11], [14], [15]. After achieving excellent agreement between experimental results and theoretical calculations, I designed a quasi-DMS WDM system propagating over 10,000 km which is an upgrade version of the single-channel setup [11]. Studies of signal dynamics as well as the multi-channel performance are presented in Chap. 5. In Chap. 6, I focus on a study that compares the signal characteristics and system performance in the Tyco-CRZ system [1], [2], the CNET-DMS system [3]–[5], and the KDD-RZ system [6]–[8]. In Chap. 7, I briefly summarize the results of my dissertation.

Chapter 2

Mathematical models

2.1 Modified NLS equations

In general, my simulation model used a modified nonlinear Schrödinger equation that may be written as

$$i\frac{\partial q}{\partial z} + \frac{1}{2}[\kappa(z) - ib(z)]\frac{\partial^2 q}{\partial t^2} + \frac{i}{6}d\frac{\partial^3 q}{\partial t^3} + |q|^2 q = ia(z)q + \hat{F}(z, t). \quad (2.1)$$

Here, the pulse envelope q is normalized as $q = E(n_2\omega_0 L_D/A_{\text{eff}}c)^{1/2}$, where E is the electric field envelope, $n_2 = 2.6 \times 10^{-16} \text{ cm}^2/W$ is the Kerr coefficient, ω_0 is the central frequency, A_{eff} is the effective area, and c is the speed of light. The quantity L_D is the characteristic dispersion length; it equals $T_0^2/|\beta_0''|$, where T_0 is a characteristic scale time, and β_0'' is the dispersion used in characteristic scaling. The distance z is normalized as $z = Z/L_D$, where Z is the physical distance. The retarded time t is normalized as $t = (T - \beta_0'Z)/T_0$, where T is the physical time and β_0' is the inverse group velocity. Other quantities are normalized as follows: $\kappa = -\beta''(z)/|\beta_0''|$, $d = -\beta_0'''T_0/|\beta_0''|$, where β_0''' is the third order dispersion, and $b(z) = B(z)L_D/T_0^2$, where $B(z)$ is the filter curvature when in-line filters are present.

The variable $a(z) = \alpha(z)/2L_D$, where $\alpha(z)$ is the power gain or loss. The net gain coefficient $a(z)$ may be written as:

$$a(z) = \begin{cases} g_m, & z_{m,r} < z < z_{m,r} + L_{\text{amp}} \\ -\Gamma, & \text{elsewhere,} \end{cases} \quad (2.2)$$

where g_m is the gain coefficient of the m -th amplifier and Γ is the loss coefficient of the fiber, while $z_{m,r}$ is the initial position of the m -th amplifier on the r -th round trip and L_{amp} is the amplifier length. The approach introduced here focuses on a loop system; however, for a straight-line system, I would set r equal to 1 and make no other changes. The autocorrelation function for the Langevin term in Eq. (2.1) may be written as:

$$\langle \hat{F}(z, t) \hat{F}^*(z', t') \rangle = 2\theta(z)g_m \frac{n_2 \hbar \omega_0^2 L_D}{A_{\text{eff}} T_0 c} \delta(z - z') \delta(t - t'), \quad (2.3)$$

where \hbar is the Plank's constant and $\theta(z)$ equals the spontaneous emission factor n_{sp} when $z_{m,r} < z < z_{m,r} + L_{\text{amp}}$ and is zero elsewhere. I solve Eq. (2.1) using a standard split-step approach.

2.2 Gain saturation model

In order to accurately calculate the evolution of the pulses in WDM systems, it is of critical importance to carefully calculate the effects of the amplifier saturation using a multiple time/length scale approach in which I average over the rapid variations of $q(z, t)$ to determine the evolution of the gain and then fix the gain to determine the evolution of $q(z, t)$ [35], [36]. If I consider the evolution of the gain coefficient of the m -th amplifier in the loop, then its gain coefficient may be written,

$$\frac{\partial g_m(\zeta, \tau)}{\partial \tau} + \frac{g_m(\zeta, \tau) - g_{m,0}}{\tau_A} = -\frac{g_m(\zeta, \tau) |q(\zeta, \tau)|^2}{U_{\text{sat}}}, \quad (2.4)$$

where $\tau = T/T_0$ is the normalized time; in contrast to t used in Eq. (2.1), τ is unretarded. The distance ζ is internal to the amplifier so that $0 \leq \zeta \leq L_{\text{amp}}$ and is normalized with respect to L_D . The quantity $g_{m,0}$ is the unsaturated gain of the m -th amplifier, τ_A is the normalized relaxation time, and U_{sat} is the saturation energy. To model the recirculating loop experiment of Jacob, et al. [11], I set τ_A equal 1 msec and U_{sat} equal 10 μ joule, corresponding to a saturation power of 10 mW.

To solve Eq. (2.1), in parallel with Eq. (2.4), I must relate ζ and τ to z and t in the m -th amplifier. I first note that $\tau = (L_D\beta'_0/T_0)z$. If the recirculating loop is short (around 100–200 km), I must take into account the transient evolution of the gain in each amplifier as well as the variation of $|q(\zeta, \tau)|^2$ as a function of position ζ inside the amplifier. However, I may assume that at a fixed value of ζ this variation is very slow. Since I only keep a limited range of τ in Eq. (2.1)—on the order of several hundred picoseconds—I may average over the rapid variations of $q(z, t)$ as a function of t to find

$$g_{m,r+1}(\zeta) = g_{m,r}(\zeta) \exp \left[-N \left(\frac{\Delta t}{\tau_A} + \frac{U_{m,r}(\zeta)}{U_{\text{sat}}} \right) \right] + g_{m,0} \frac{\Delta t}{\tau_A} \frac{1 - \exp \left[-N \left(\frac{\Delta t}{\tau_A} + \frac{U_{m,r}(\zeta)}{U_{\text{sat}}} \right) \right]}{\frac{\Delta t}{\tau_A} + \frac{U_{m,r}(\zeta)}{U_{\text{sat}}}}, \quad (2.5)$$

where N pulses fill the loop with pulses separated in time by Δt so that $\Delta z = (T_0/L_D\beta'_0)N\Delta t$ is one round trip in the loop in normalized units. The integer r indicates the number of round trips so that $z = z_{m,r}$ is the z -coordinate of the entry to the m -th amplifier on the r -th round trip, and

$$g_{m,r}(\zeta) = g_m \left[\tau = (L_D\beta'_0/T_0)z_{m,r}, \zeta \right]. \quad (2.6)$$

Finally, the energy $U_{m,r}(\zeta) = \langle |q(z_{m,r} + \zeta, t)|^2 \rangle \Delta t$ corresponds to the average energy

in a single bit at $z = z_{m,r} + \zeta$. Having at each ζ determined the slow variation of the gain from Eq. (2.5), I then determine the fast variation of $q(z, t)$ from Eq. (2.1) by assuming that the gain is independent of t on each round trip. I have found that dividing the amplifier into 100 sections yields a sufficiently accurate numerical solution for $g_{m,r}(\zeta)$. I note that in steady state, Eq. (2.5) becomes

$$g_{m,r+1}(\zeta) = g_{m,r}(\zeta) = \frac{g_{m,0}}{1 + \frac{\tau_A}{\Delta t} \frac{U_{m,r}(\zeta)}{U_{\text{sat}}}}, \quad (2.7)$$

where $U_{m,r}(\zeta)$ is constant as a function of r . To obtain accurate results for the convergence of initial pulse shapes to their final values, one must use Eq. (2.4) to simulate the saturation of the erbium doped fiber amplifier (EDFA) in the short loop cases; however, for a longer loop (longer than 200 km), I prefer to use the steady state solution of Eq. (2.7) because the round trip time of the signal propagation is longer than the relaxation time τ_A of the EDFA so that I can assume the EDFA has reached its steady state.

2.3 Scale length

Previous studies [29], [36] show that the signal behavior in a given transmission system can be characterized by the ratio of the transmission distance over the nonlinear length, and the dispersion length. These theories indicate that the pulse behavior will be dominated by the dispersion when the transmission distance is larger than the dispersion length. Similarly, one could expect a significant influence of the nonlinearity in a system when the ratio of the total transmission distance to the nonlinear length is comparable. The dispersion length and the nonlinear length are related to the pulse duration and the pulse peak power, as well as the path dispersion. In most modern

systems, none of these parameters is fixed during the transmission. Hence, I define an effective nonlinear length as well as the effective dispersion length as follows.

The average dispersion over a single map period is defined as $\overline{D} = (D_1 L_1 + D_2 L_2)/(L_1 + L_2)$ and $\overline{\beta}'' = (\beta_1'' L_1 + \beta_2'' L_2)/(L_1 + L_2)$ where D_1 or β_1'' is the dispersion of fiber segment 1 with the length of L_1 and D_2 or β_2'' corresponds to the dispersion of fiber segment 2 with a length of L_2 . We measure D_j in units of ps/nm-km, and it is positive in the anomalous dispersion region, while we measure β_j'' in the units of ps²/km and it is positive in the normal dispersion region. The residual average dispersion over the transmission distance L_T is given by $\delta\overline{D} = \int_0^{L_T} D(z)dz/L_T$ and $\delta\overline{\beta}'' = \int_0^{L_T} \beta''(z)dz/L_T$. I now define the effective dispersion length as $L_{D,\text{eff}} = T_{\text{min}}^2/|\overline{\beta}''|$, where T_{min} is the minimum pulse duration at the end of the transmission line. We also define the effective nonlinear scale length as $L_{\text{NL,eff}} = 1/(\gamma\overline{P}_0)$ with the path average pulse intensity $\overline{P}_0 = \int_0^{L_T} P_0(z)dz/L_T$, where the variable $P_0(z)$ corresponds to the peak power of the pulse along the transmission, and the nonlinear coefficient γ equals $n_2\omega_0/cA_{\text{eff}}$. I now define $\gamma_{\text{NL}} = L_T/L_{\text{NL,eff}}$ and $\gamma_{\text{D}} = L_T/L_{D,\text{eff}}$. I will use these two ratios to characterize the signal propagation [36].

2.4 Evaluation of the system performance

The evaluation of the system performance will focus on determining the timing jitter and the amplitude jitter. I will include ASE noise using the Monte Carlo method [35]. To calculate the timing jitter, I define the central pulse time position t_p [37] as

$$t_p = \frac{1}{U} \int_{-\infty}^{\infty} t |q(t)|^2 dt, \quad (2.8)$$

where $U = \int_{-\infty}^{\infty} |q(t)|^2 dt$ is the pulse energy. Hence, the timing jitter is defined as

$$\delta t = [\langle t_p^2 \rangle - \langle t_p \rangle^2]^{1/2}. \quad (2.9)$$

The simulator includes an electrical 5-th order Bessel lowpass filter to match the receiver. The amplitude jitter is evaluated using a Q factor that is calculated in turn from the electrical current at the receiver, with $Q = (\mu_1 - \mu_0)/(\sigma_1 + \sigma_0)$, where, as usual, the variables μ_1 and μ_0 are the means of the marks and the spaces, while σ_1 and σ_0 are the standard deviations of the marks and spaces respectively. I then set the following two conditions as the criteria for an acceptable system performance: (1) $Q \geq 6$ corresponding to a BER induced by the amplitude jitter less than 10^{-9} and (2) $\delta t \leq 5.8$ ps corresponding to a BER induced by the timing jitter less than 10^{-9} with a detection window of 50 ps.

Chapter 3

Study of the timing jitter in a DMS system—validation of the ASE model

The invention of the EDFA revolutionized the development of fiber communications systems, leading directly to the advent of WDM and Terabit communications. However, these amplifiers allow fiber impairments to accumulate over distance of several hundred kilometers in terrestrial systems and several thousand kilometers in transoceanic systems. It has been recognized that optical fiber impairments—including ASE noise produced by optical amplifiers—will ultimately limit the achievable data rate in a very complex way. Nonlinearity and chromatic dispersion interact with ASE noise to degrade the signal-to-noise ratio (SNR) at the receiver as well as to induce timing jitter. In order to obtain a reliable numerical model of a real fiber communications system, it is important to create a complete simulator that can accurately simulate the details of the dispersion map, the interaction between the signal and the noise, the nonlinear interaction between two signal pulses, and the influence of chromatic dispersion simultaneously. To build such a simulator, an accurate ASE module is of great importance.

It is well known that ASE noise at the EDFAs can be treated as Gaussian white noise. Thus, I modeled its effects by adding noise in the Fourier domain after each amplifier. Writing the Fourier transform of the noise field as $\delta\tilde{q}(z, \omega)$, the real $\delta\tilde{q}_{\text{re}}$ and imaginary $\delta\tilde{q}_{\text{im}}$ components of $\delta\tilde{q}$ are Gaussian-distributed random variables with zero means and variances given by $A^2/2$, where $A = [(G - 1)n_{\text{sp}}n_2\hbar\omega^2L_D\Delta\nu/A_{\text{eff}}T_0c]^{1/2}$, $G = \exp\left[\int_0^{L_{\text{amp}}} 2g(z)dz\right]$ is the gain associated with the amplifier, and $\Delta\nu$ is the normalized bandwidth associated with each component. Alternatively, one can add an amount of noise $\delta\tilde{q} = A\exp(i\varphi)$ to each Fourier component, with φ being a random phase uniformly distributed between 0 and 2π . While the second approach is not strictly correct, the large number of Fourier modes coupled with the central limit theorem imply that the results should be the same. Numerical experimentation that I have done has shown that using the two approaches described here leads to the same results as long as the correct amount of noise power is added on average to each Fourier component.

Using the Monte Carlo method, I demonstrated the reliability of this ASE noise module by studying the timing jitter effect in a DMS transmission system [37]. I used a dispersion map that consisted of alternating 100 km spans of positive and negative dispersion, and I injected a chirp-free DMS pulse at the mid-point of the negative dispersion segment with a FWHM duration t_{FWHM} equal to 20 ps. Fiber loss was 0.21 dB/km with an amplifier spacing of 50 km. The fiber effective area A_{eff} was $50 \mu\text{m}^2$, and the spontaneous emission factor n_{sp} was 2.0. I set the path average dispersion $\bar{\beta}'' = -0.1 \text{ ps}^2/\text{km}$ or $\bar{D} = 0.08 \text{ ps}/\text{nm}\cdot\text{km}$, while the normalized path average dispersion $\bar{\kappa} = 1$ with the choice of $\beta_0'' = -0.1 \text{ ps}^2/\text{km}$. In the first set of simulations shown in Fig. 3.1, I chose the local dispersion $\beta_1'' = -3.0 \text{ ps}^2/\text{km}$ and hence $\beta_2'' = 2.8 \text{ ps}^2/\text{km}$. The parameter used to characterize the strength of the dispersion

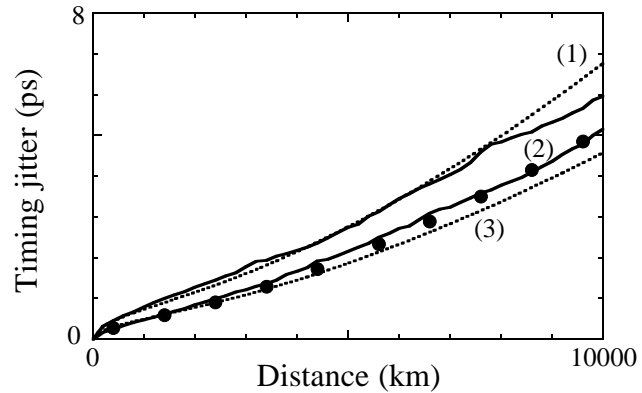


Figure 3.1: The timing jitter as a function of distance with amplifiers spaced 50 km. The curves (1) correspond to the timing jitter in a standard soliton system with uniform dispersion fiber. The dashed line is the analytical result from Gordon-Haus theory [16], while the solid line shows the result of the Monte Carlo simulations. Curve (2) corresponds to the timing jitter in a dispersion-managed soliton system. The circles show the result of the semi-analytical approach [17], while the solid line shows the result of the Monte Carlo simulations. Curve (3) shows the modified Gordon-Haus result [18]

management can be written as $\gamma_{\text{map}} = 2[(\beta_1'' - \overline{\beta''})L_1 - (\beta_2'' - \overline{\beta''})L_2]/t_{\text{FWHM}}^2$, where L_1 and L_2 are the span lengths of 50 km in the dispersion map, and t_{FWHM} is the FWHM pulse duration as one can recall. In this first set of simulations, I found that γ_{map} is 2.9, corresponding to an energy enhancement factor of 2.17. The enhancement factor is defined as the ratio of the actual DMS pulse energy found numerically in the simulation to the standard soliton energy in the uniform dispersion map in which $\kappa(z) = 1$. Figure 3.1 shows the timing jitter as a function of distance, where the solid lines represent the average of 100 Monte Carlo simulations with exactly the same simulation parameters. The timing jitter was calculated using the definition in Eqs. (2.8) and (2.9) as in Chap. 2.

The comparison of the Monte Carlo results to the modified Gordon-Haus theory [13], [31], indicates that the reduction of the timing jitter in a DMS system is less than predicted, and the deviation grows with the distance. Figure 3.2 shows what happened when I put the amplifiers at the points of greatest pulse expansion in the dispersion map and increased the space between the amplifiers to 100 km. Keeping \overline{D} the same as in the previous case and $\gamma_{\text{amp}} = 3.65$, I found that the deviation from the modified Gordon-Haus theory differed by a large percentage—increasing to 30% after 10,000 km. The time-bandwidth product for this case is 0.66, and the enhancement factor equals 8.16. Extensive simulations show that as the time-bandwidth product increases, the predictions of the modified Gordon-Haus theory consistently become worse. This result is intuitively reasonable since the larger spectrum implies that the stable pulse can “grab” more noise. I also directly calculated the timing jitter using a semi-analytical approach [17] developed by our former group member Dr. Grigoryan. The results are in complete agreement with the Monte Carlo simulations.

Furthermore, I compared the results of Monte Carlo simulations with the Gordon-

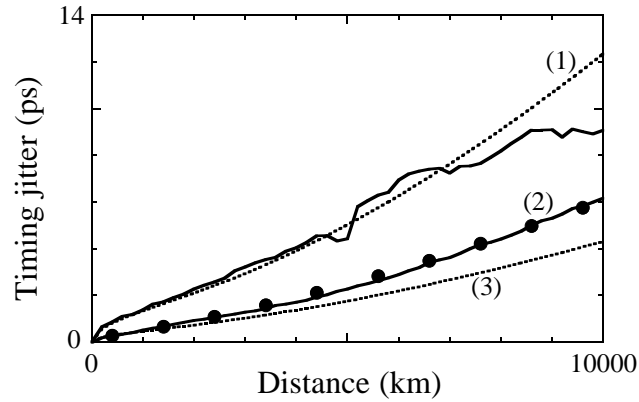


Figure 3.2: The timing jitter as a function of distance with amplifiers spaced 100 km and put at the points of maximum pulse expansion in the dispersion map. The curves (1), (2), and (3) are as in Fig. 3.1.

Haus theory [16] in a uniform dispersion fiber with the same path average dispersion. I found that numerical simulations are only consistent with the Gordon-Haus theory within 8,000 km in the case of Fig. 3.1. Beyond that, a considerable discrepancy between the Gordon-Haus theory and my simulations appears because linearization is no longer valid; in the case of Fig. 3.2, this discrepancy occurs even sooner. However, the linearization reminds valid for the dispersion managed solitons up to 10,000 km because their larger intensity leads to a higher SNR so that the pulse profiles $q(t)$ acquired numerically were less influenced by the accumulation of ASE noise.

Chapter 4

Comparison between theory and experiment for a single channel DMS system in a recirculating loop

A number of investigations have been carried out considering the interaction of signal and noise or the interaction of signals with each other in a DMS system [38]–[47]. However, it is difficult to use this previous work to analyze or optimize a real experimental implementation of a DMS system because in any real systems these effects occur simultaneously and interact with each other. During the second stage of my thesis study, with the collaboration of my colleagues, I implemented a system model that accurately predicts the behavior of a recirculating loop experiment. Using this model, I elucidated the principal source of errors and show specifically that (1) the principal source of errors is the growth of ASE noise in the spaces, (2) gain saturation in the amplifier plays an important long-term role in stability but nonlinear polarization rotation does not. The theoretical prediction of the system performance is in excellent agreement with the experimental measurements.

4.1 System setup

The recirculating loop system that I studied was built at Laboratory for Physical Sciences and was used to transmit single-channel DMS pulses at 10 Gbit/s [11], [14]. I show a schematic illustration of the recirculating loop in Fig. 4.1. There are four spans of dispersion-shifted fiber (DSF), each about 25 km in length, with a normal dispersion D_1 equal to -1.10 ps/nm-km at 1551 nm, followed by an approximately 7 km span of standard single mode fiber (SMF) with an anomalous dispersion D_2 equal to 16.6 ps/nm-km at 1551 nm [11]. The dispersion slope is 0.075 ps/nm²-km. An amplifier follows each span of normal dispersion fiber and a fifth amplifier follows the 2.8 nm bandpass filter that is at the end of the 7 km span of standard fiber. The total loss within one loop period is 31.53 dB, including the loss in the fibers, the optical filter, connectors, couplers, and acousto-optic switches. I also defined the total unsaturated gain coefficient within one loop period as $G_0 = \exp \left[\sum_{m=1}^5 \left(2 \int_0^{L_{\text{amp}}} g_{m,0} dz \right) \right]$ that can be altered by changing the individual unsaturated gain coefficient $g_{m,0}$ at each amplifier. In my investigation, I always set $\exp(2g_{m,0}L_{\text{amp}}) = G_{a,0}$, ($m = 1 \dots 4$) the same and set $\exp(2g_{5,0}L_{\text{amp}}) = G_{b,0}$ a little larger in order to compensate for the loss in the switches, the optical filter, and the couplers. The value of G_0 will determine the energy of the DMS pulse in the steady state. The injected initial pulse train takes the form of 1-1-1-0-0-0-1-0 which includes all possible nearest-neighbor interactions since only the nearest-neighbor interactions are important for single-channel DMS systems. The calculation window is 800 ps corresponding to a 10 Gbit/s signal, so that the pulse train that I used is in effect repeated periodically *ad infinitum*. Equations (2.1)–(2.5), along with the initial condition just specified, comprise the model of our recirculating loop experiments.

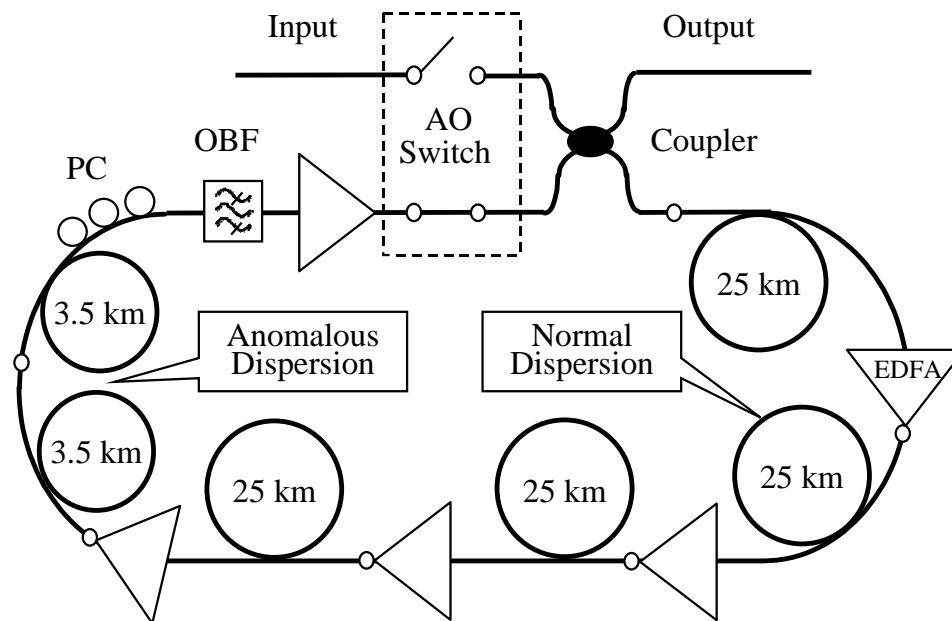


Figure 4.1: The experimental setup for the 10 Gbit/s DMS transmission over 24,500 km [11]. Small circles along the loop show the tap points at which experimental data could be extracted.

4.2 Dynamics of Dispersion Managed Solitons

The first issue in this portion of my work is the dynamic behavior of the DMS pulses in the system. As a consequence of gain saturation and filtering, initial pulse trains with varying pulse shapes and pulse power within a sizeable range eventually reach the same steady state in the system. This result is consistent with our experiments that show that the DMS behavior is independent of the input parameters over a wide range [14]. However, if the gain saturation is neglected, the initial pulse shapes that are launched into the system must be very close to the final periodically-stationary pulse shapes in order for the system to converge; this sensitivity is in contradiction to the experiments. This point is illustrated in Fig. 4.2 in which I show the evolution of the peak power of a Gaussian-shaped pulse as I vary the round trip gain G_0 and the peak power of the input pulse P_{in} . In the cases (a), (b), and (c) shown in Fig. 4.2, in which the gain saturation is turned off, the system has difficulty stabilizing. In cases (a) and (c) the pulses are overamplified so that the amplitudes of the pulses continually increase and eventually blow up. In case (b), the pulses are under-amplified and eventually disappear. By contrast in cases (d) and (e) in Fig. 4.2, in which gain saturation is included, the pulses ultimately stabilize with the same pulse shape, regardless of the details of the input pulse shapes.

Once I achieved stable pulse propagation in the system, I next considered the detailed dynamics of the DMS pulse after the system had reached its steady state. In Fig. 4.3(a), I directly compare the experimentally-measured full width at half maximum (FWHM) pulse durations to our simulation results at the taps shown in Fig. 4.1. Note that the horizontal scale is expanded in the anomalous dispersion regime for better visibility. Agreement between our experiments and our simulations

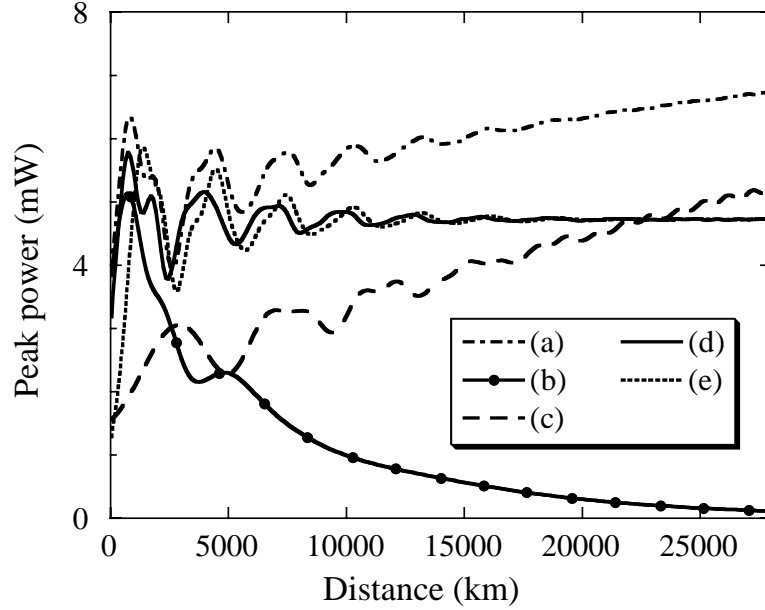


Figure 4.2: The influence of different gain models on the stabilization of the DMS pulse propagation with $\bar{D} = 0.02$ ps/nm-km. (a) Without gain saturation, $G_0 = 31.6$ dB with $G_{a,0} = 5.0$ dB and $G_{b,0} = 11.6$ dB, and $P_{\text{in}} = 9$ dBm. (b) Without gain saturation, $G_0 = 31.5$ dB with $G_{a,0} = 5.0$ dB and $G_{b,0} = 11.5$ dB, and $P_{\text{in}} = 9$ dBm. (c) Without gain saturation, $G_0 = 31.6$ dB with $G_{a,0} = 5.0$ dB and $G_{b,0} = 11.6$ dB, and $P_{\text{in}} = 5$ dBm. (d) With gain saturation, $G_0 = 32.45$ dB and $P_{\text{in}} = 9$ dBm. (e) With gain saturation, $G_0 = 32.45$ dB and $P_{\text{in}} = 5$ dBm. In cases (d) and (e), $G_{a,0} = 5.4$ dB, and $G_{b,0} = 10.85$ dB.

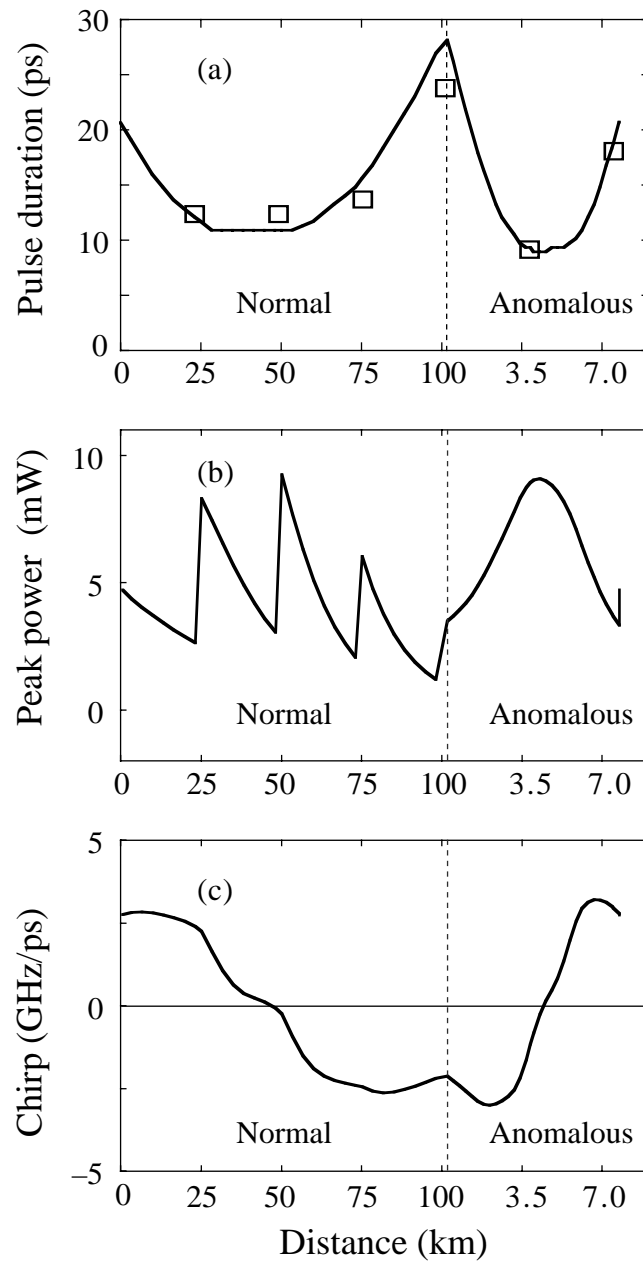


Figure 4.3: The dynamics of the DMS signal at steady-state. I show the (a) duration, (b) peak power, and (c) the chirp of the pulse as functions of distance during one round trip in the loop. The squares show the experimentally measured pulse durations.

is excellent. In Fig. 4.3(b) and 4.3(c), I show the variation of the pulse peak power and the chirp as a function of position along the loop. Here, I define the chirp as the negative of the second derivative of the phase with respect to time at the central position of the pulse in the time domain. Despite the asymmetric variation of the pulse peak power, the chirp goes nearly to zero at the midpoints of both the anomalous and normal dispersion spans just as in the lossless, unfiltered case [48]. Extensive study shows that third order dispersion, pulse interaction, and nonzero saturable absorption play insignificant roles in this system.

4.3 System Performance in the Presence of Amplified Spontaneous Emission Noise

Now I compare simulation results to those obtained in [11] considering the contribution of the ASE noise. Using Eq. (2.9), I first calculated the timing jitter using 100 different realizations of the ASE noise for both $\overline{D} = 0.08$ ps/nm-km and $\overline{D} = 0.04$ ps/nm-km. I set $G_0 = 33.6$ dB with $G_{a,0} = 5.8$ dB and $G_{b,0} = 10.4$ dB for $\overline{D} = 0.08$ ps/nm-km, and I set $G_0 = 33.2$ dB with $G_{a,0} = 5.8$ dB and $G_{b,0} = 10.0$ dB for $\overline{D} = 0.04$ ps/nm-km. The results are shown in Fig. 4.4. The agreement between experiment and simulation is good considering the 0.5 ps uncertainty in the measurements. As expected, the timing jitter is smaller for smaller values of \overline{D} , and the growth rate of the jitter is smaller than the standard Gordon-Haus rate ($\propto Z^{3/2}$) due to the addition of the optical filter. For our 10 Gbit/s system I estimate that a timing jitter of 5.8 ps will lead to an error rate of 1×10^{-9} with the detection window of 50 ps. Since the maximum timing jitter is well below 5.8 ps even with $\overline{D} = 0.08$

ps/nm-km, timing jitter does not limit our system.

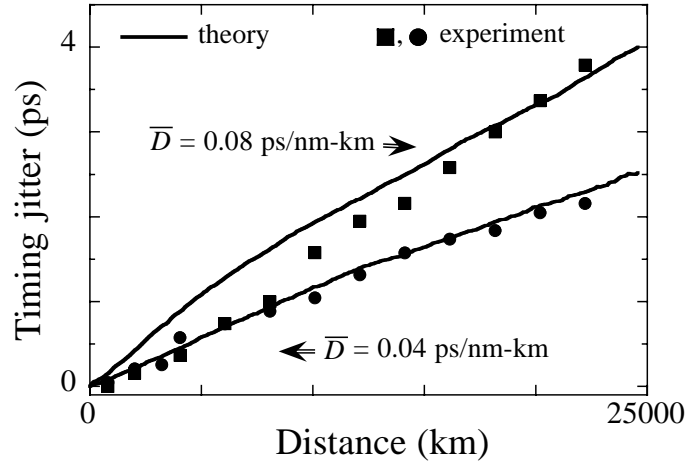


Figure 4.4: Timing jitter as a function of the transmission distance in a single channel experiment.

Assuming that the fluctuations are Gaussian-distributed in both the marks and spaces [49], I could then calculate the amplitude margin at a given error rate of 1×10^{-6} which is the value used in our experiments [11]. The margins are expressed as the voltage decision levels once the signal has passed through the receiver. The bandwidth of the lowpass electrical filter is set to 4.3 GHz to match the receiver in the experiment. The assumption that the distribution of the marks and spaces about their means is Gaussian is also questionable. Indeed, this assumption is known to fail far out on the tails of the distribution functions [49]. However, this assumption yields excellent agreement between the experiments and simulations, indicating that higher-order effects are not important at the error rates that I am considering. Figure 4.5 shows the comparison of the simulations and experiments when $\bar{D} = 0.08$ ps/nm-km and $\bar{D} = 0.04$ ps/nm-km. The only parameters that I changed are $G_0 = 33.65$ dB with $G_{a,0} = 5.8$ dB and $G_{b,0} = 10.45$ dB in first case and $G_0 = 33.3$ dB in the second

case with $G_{a,0} = 5.8$ dB and $G_{b,0} = 10.1$ dB. The upper curves show the margin for the marks, and the lower curves show the margins for the spaces. Figure 4.5 shows that while the margins for the marks undergo a slow, almost linear decay, the margins for the spaces grow nearly exponentially. This behavior is a well-know consequence

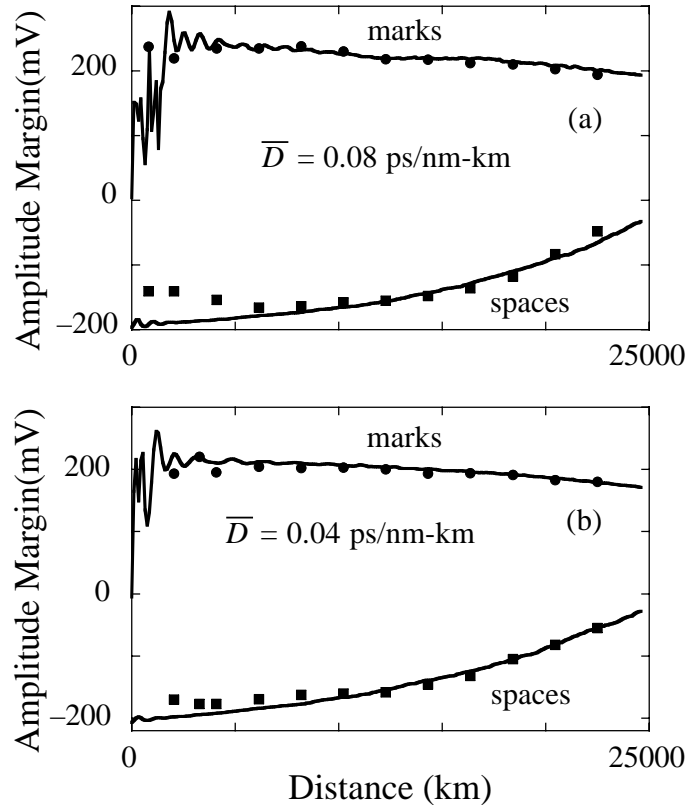


Figure 4.5: Amplitude margin along the transmission line at a bit rate of 10 Gbit/s. The upper curve shows the decision level of the marks, and the lower curve shows the decision level of the spaces. Squares and circles are the experimental data.

of including a filter in the loop. After a detailed study of the growth of the variation of the marks and the spaces, I then concluded that the buildup of the ASE noise in the spaces limits the transmission distance in our system.

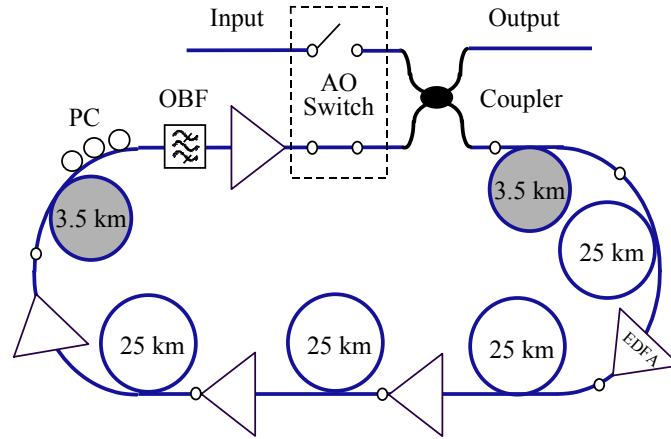


Figure 4.6: The experimental setup for the 20 Gbit/s DMS transmission [15]. The white circles represent the normal dispersion fiber while the gray ones correspond to the anomalous fiber.

Later the system was upgraded by Dr. Carter and his colleagues to a 20 Gbit/s single channel DMS system propagating over 20,000 km [15], that yielded the world record for a single channel DMS transmission at 20 Gbit/s. The experimental setup is similar to the 10 Gbit/s system except that the SMF span was equally split into two pieces, and one of them was moved to the front of the first normal DSF span shown in Fig. 4.6. The reason behind this adjustment is that in the midpoint of the anomalous span (SMF segment) the pulse profile is close to the transform-limited Gaussian pulse. Hence, when a Gaussian pulse was initially injected at this point in the dispersion map, it would significantly reduce the initial transient regime. Again, the predictions of my simulation agreed with the experimental measurements very well. The results of the system margins are shown in Fig. 4.7 with $\bar{D} = 0.03$ ps/km-nm and an average power of 2.0 mW.

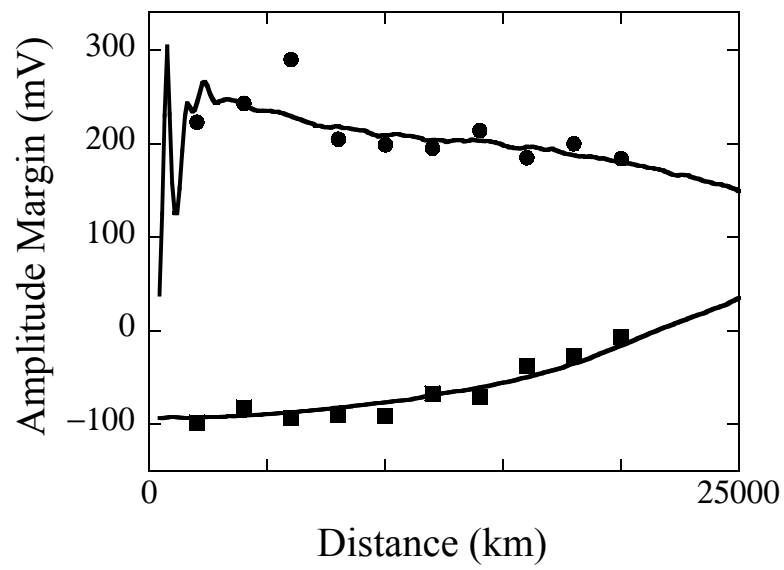


Figure 4.7: Amplitude margin along the transmission line at a bit rate of 20 Gbit/s. Solid lines are simulation results while squares and circles corresponding to the experimental data.

Chapter 5

Testing the feasibility of a 4×10 Gbit/s WDM system using a periodically stationery DMS format

Optical networking began with a few very simple and basic concepts and has evolved dramatically toward solving the real-world problems of building large-scale networks that are robust against failure and traffic surges. The major challenge to all those working in optical communications, communications in general, and in optical networking in particular, is to find the most practical way of driving down the cost of that bandwidth. Increasing the channel count is a promising approach to enhance the system capacity; however, it has been proved that raising the signal bit rate per channel is more cost effective than simply increasing the channel count in order to catch up to the demands of the growth of network capacity. The cost of commercial WDM systems at a signal rate of 10 Gbit/s is only twice as expensive as 2.5 Gbit/s WDM systems; however the capacity increases four times. It has been predicted that 40 Gbit/s WDM systems will only raise the cost by a factor of 2.5 compared to

10 Gbit/s systems. Hence, it will be of great interest to study WDM systems with a signal bit rate over 10 Gbit/s. It has also been discovered that WDM systems are not limited by the flat-gain bandwidth of EDFAs—since there are many so-called “super amplifiers” that have been developed [50], [51], but it is the nonlinear interaction due to the Kerr effect among the channels, as well as the constraints set by the dispersion slope and the polarization mode dispersion (PMD) [52].

Concerning these challenges, solitons nevertheless would appear to have certain fundamental advantages. First among these is that, for solitons, the phase shifts from self-phase modulation and from chromatic dispersion periodically cancel each other, with the consequence that neither spectral nor temporal broadening can accumulate [53]. Thus lumped elements to cancel the path-average dispersion are not required for solitons. Dispersion compensation is difficult to use in networks since the amount needed is specific to each channel and each distance, and both may not be known. Second, for a proper choice of the dispersion map, solitons can be made to exhibit a nearly perfect transparency to each other during the collisions which occur in a WDM system. Finally, only solitons can exist in the presence of guiding filters and thus benefit from the regeneration, the automatic gain leveling, and the tolerance of collision-induced-timing shifts that guiding filters provide.

As I described in Chap. 4, Dr. Carter and his colleagues have built a unique single-channel DMS transmission testbed, which they used to demonstrated a world record transmission distance for single channel DMS pulse propagation at 20 Gbit/s [15]. It is natural to explore the possibility of upgrading this single channel experiment into a WDM system. It is also of great interest to build a flexible experimental tool that allows us to easily adjust the power level as well as the dispersion map structures in the system so that one can propagate different pulse formats in the same testbed. In

this way, one can obtain physical insight into the pulse behaviors in different systems.

5.1 Primary system design

The primary design of a 4×10 Gbit/s WDM system that would satisfy this requirement is shown in Fig. 5.1. It is based on a recirculating loop with an expanded loop length on the order of 500 km, which will eliminate the problems that were observed when we were using a short-length loop, such as the influence of transient gain saturation on in-line EDFAs [35] and noise co-polarization with the signal due to strong and highly repeatable polarization dependent loss [54]. There are five identical dispersion map periods in the loop. Each of them is the same as in the single channel system described in Chap. 4 but with the launching point moved to the middle of the anomalous span. There are two amplifiers evenly located inside each map with a spacing of 53 km, which, according to my numerical experiments, is the longest amplifier span that one could use in this configuration. Instead of inserting an optical bandpass filter in each round trip of the loop, I introduced a dispersion slope compensator (DSC) in the loop to individually balance the residual dispersion of each channel due to the dispersion slope so that the balance of dispersion and nonlinearity could be satisfied at each individual channel. Inside the DSC, there is a multiplexer/demultiplexer (MUX/DEMUX) pair with a super-Gaussian filter shape to combine or separate the channels. Two pieces of SMF and two pieces of DCF fiber followed by amplifiers or attenuators are placed at the output ports of the demultiplexer to compensate the accumulated dispersion for each channel. Consequently, this kind of DSC can be easily modified by replacing the SMFs and DCFs as required. The amplifiers and attenuators in the DSC also provide gain slope compensation over

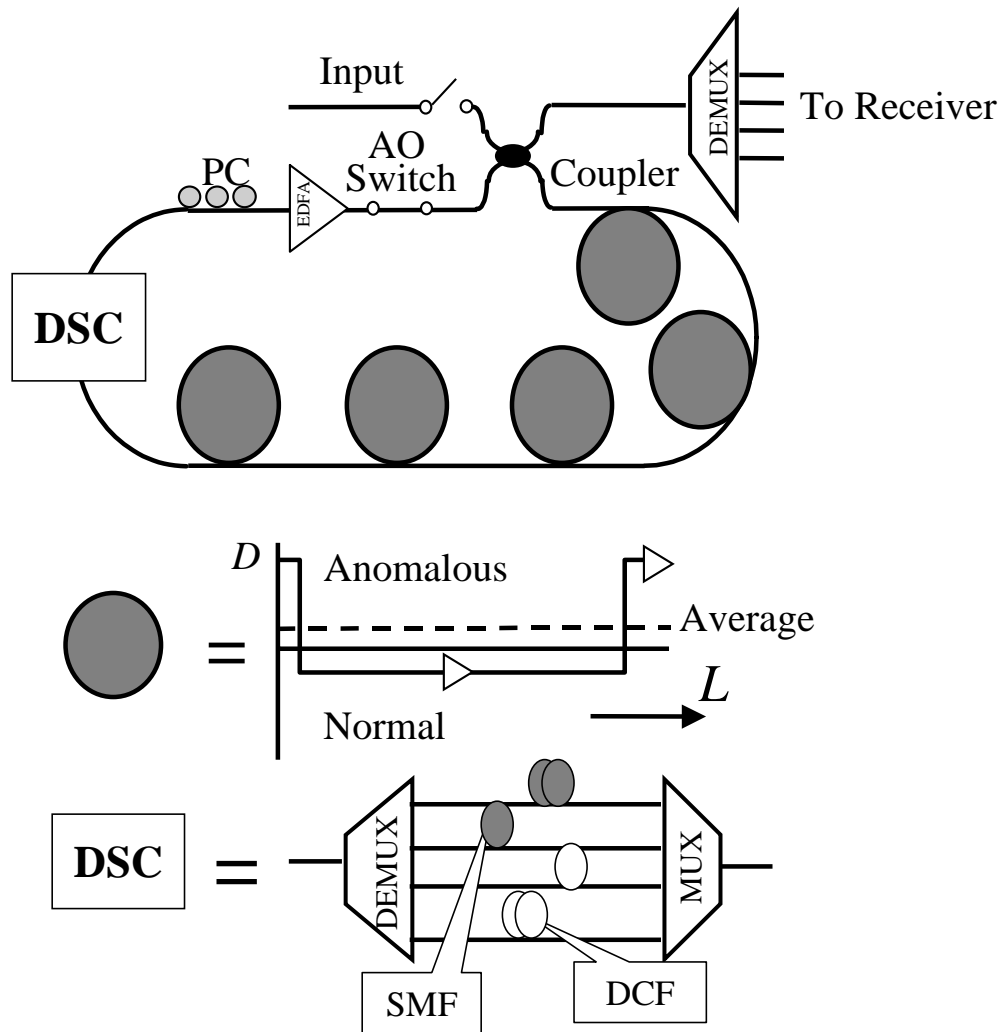


Figure 5.1: A 4×10 Gbit/s experimentally scaled WDM transmission system, where the dispersion slope compensator (DSC) includes a MUX/DEMUX pair with single mode fiber, dispersion compensating fiber and EDFAs.

all the channels. In addition, the MUX/DEMUX elements act as filters that play an important role in the system. The bandwidth of the MUX/DEMUX in each channel is about 0.35 nm, and the total insertion loss is 10 dB. This kind of DSC would be suitable for CRZ and RZ pulse propagation, as well as DMS propagation, with an appropriate modification of compensating fibers and launch powers. Hence, it would be possible to compare the DMS and CRZ modulation formats based on nearly the same experimental setup because of the flexibility in the power adjustment as well as the dispersion compensation.

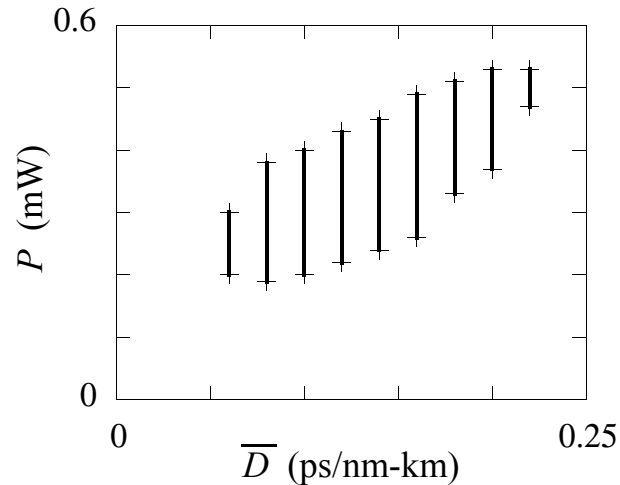


Figure 5.2: The power margins as a function of path average dispersion \bar{D} at 1.551 μm .

The remaining questions in the system design are how to choose the map dispersion as well as the pulse power. To find the answer, I searched the possible combinations for values that would achieve Q values at the end of 10,000 km single channel transmission that are larger than 6. Figure 5.2 shows the power margin and corresponding map average dispersion from 0.06 ps/nm-km to 0.2 ps/nm-km. The optimal combination that I found corresponded to setting the average dispersion \bar{D} equal to 0.1 ps/nm-km

at 1551 nm, while keeping the average power at 0.25 mW per channel. The error-free transmission distance that I calculated for a four-channel WDM system was over 10,000 km.

5.2 Nonlinear pulses propagation

Focusing first on the signal dynamics, I studied a single channel system without consideration of the ASE noise. The initial signal is a 64 bit pseudo-random string in which each pulse has a Gaussian shape and a FWHM of 12 ps. As shown in Fig. 5.3, the pulse shapes at the end of each loop cycle are periodic after passing through an initial transient regime. This behavior can be understood as a consequence of the

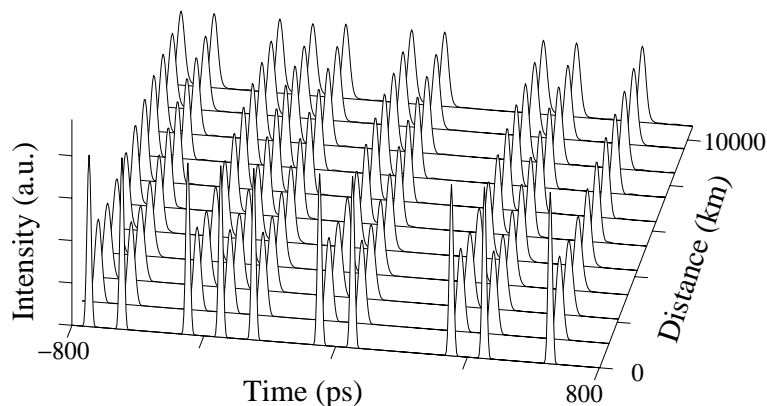


Figure 5.3: Pulse propagation of a single channel using the transmission setup shown in Fig. 5.1

complete compensation of the third order dispersion in each round trip, while the nonlinearity and chromatic dispersion balance each other in steady state. However,

inside one loop cycle, pulses breathe along the dispersion map with increased stretching factors because of the residual unbalanced dispersion due to the dispersion slope shown inside one loop period in Fig. 5.4. In other words, the system is periodically

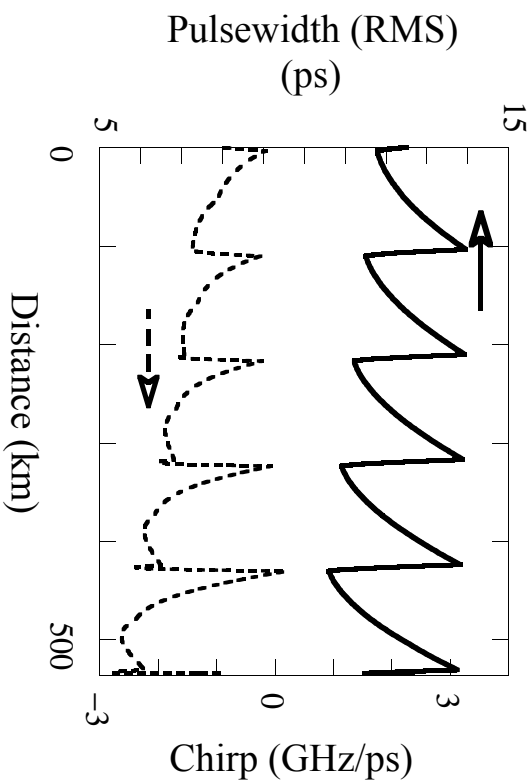


Figure 5.4: Pulse breathing inside one loop period at the steady state.

The solid line represents the evolution of the pulse duration, and the dashed line represents the variation of the pulse chirp.

stationary over five periods of the dispersion map, rather than one. Therefore, I refer to this system as a quasi-DMS system. In order to reduce the influence of the dispersive wave residue inside each pulse, I calculated the root-mean-square (RMS) of pulse duration and bandwidth instead of the full-width-half-maximum (FWHM) duration using the definitions

$$\langle t \rangle = \frac{\int t |q(t)|^2 dt}{\int |q(t)|^2 dt}, \quad (5.1)$$

$$\langle f \rangle = \frac{\int f |\tilde{q}(f)|^2 df}{\int |\tilde{q}(f)|^2 df}. \quad (5.2)$$

An interesting but not surprising phenomenon observed in the study is the evolution of the pulse spectrum shown in Fig. 5.5. Because of the cascaded filtering

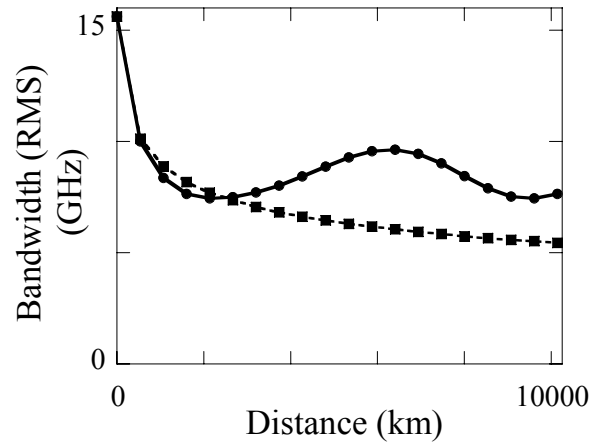


Figure 5.5: Evolution of the pulse RMS spectral intensity. The dashed line with filled squares represents the spectral evolution in a linear system

resulting from the MUX/DEMUX pair, one would expect, in a linear system, that the bandwidth of the pulses would decrease proportional to the square root of the distance. However, in this system, the self-phase modulation is able to generate new frequencies that compensate for the filtering, as shown in Fig. 5.6. Thus the nonlinearity plays a critical role in maintaining the pulse spectrum, and, hence, the periodically stable pulse propagation in the time domain.

The time-bandwidth production shown in Fig. 5.7 indicates that the final pulse shape is close to a Gaussian but with a bit of chirp.

In the last part of the single channel study, I examine the influence of the ASE noise in the signal propagation. Generally, the pulse behavior does change significantly; however, I observed both amplitude and timing jitter in the eye diagram, shown in Fig. 5.8, after 10,000 km transmission.

Figure 5.9 shows the power margin when perturbing the signal power around the

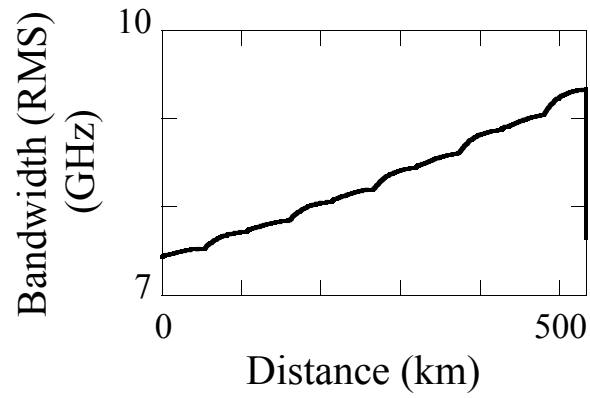


Figure 5.6: The growth of the pulse RMS duration in the frequency domain inside one loop period.

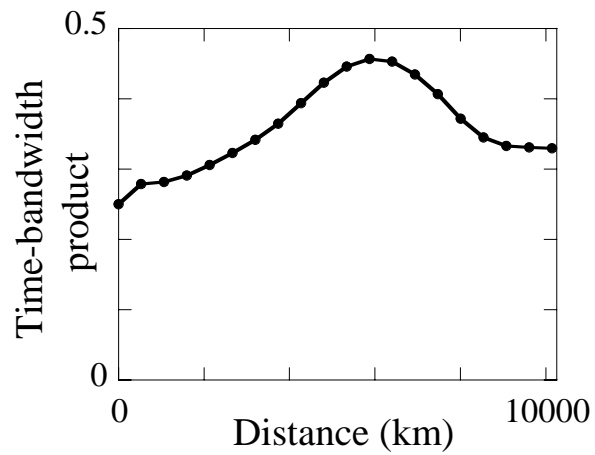


Figure 5.7: The evolution of the pulse time-bandwidth product along the transmission.

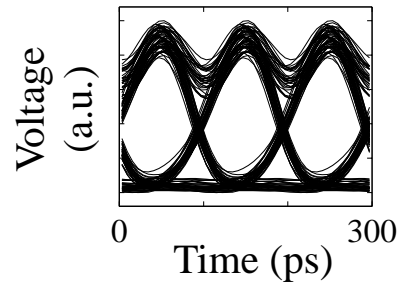


Figure 5.8: The received eye diagram for the single channel propagation.

optimal operation condition described in Sec. 5.1. The power margin corresponding to a given map average dispersion \bar{D} is quite limited. Soliton theory requires a fixed relationship between pulse energy and the dispersion in order to achieve a perfect balance of nonlinearity and chromatic dispersion. This restriction is somewhat

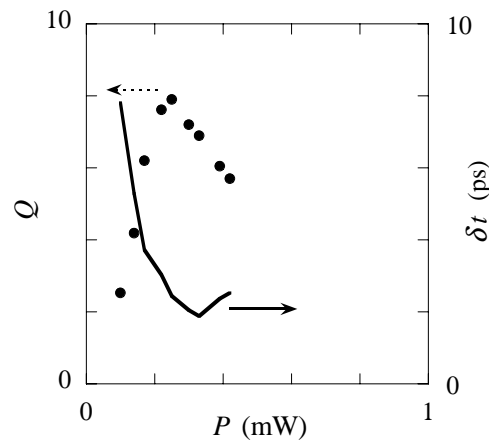


Figure 5.9: The power margin in the single channel case.

loosened with the DMS format; however, the required close relationship between \bar{D} and the pulse power is still a major limitation of these systems. Consequently, the implementation of the DMS format in a WDM system would require precise control of the signal power as well as compensation of the dispersion slope. Note that the

narrowing of the pulse spectrum visible in Fig. 5.10 at the output of the transmission, which also can be observed in Fig. 5.5, is a consequence of repeated passage of signals

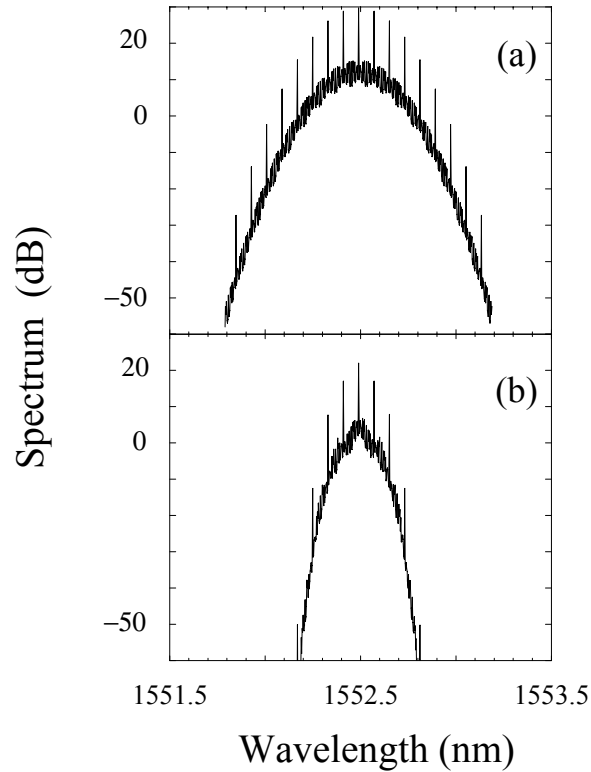


Figure 5.10: The evolution of the signal spectrum. While (a) represents the input and (b) corresponds to the output.

through the MUX/DEMUX pair. The cascading in-line MUXs and DEMUXs results the cascaded filtering that leads to the narrowing of the pulse spectrum.

5.3 Evaluation of multi-channel performance

The evaluation of the WDM system performance was carried out by launching four-channel WDM signals with a channel spacing of 0.5 nm. The evolution of the signal

spectrum is shown in Fig. 5.11. The eye diagrams after 10,000 km propagation of all channels are shown in Fig. 5.12.

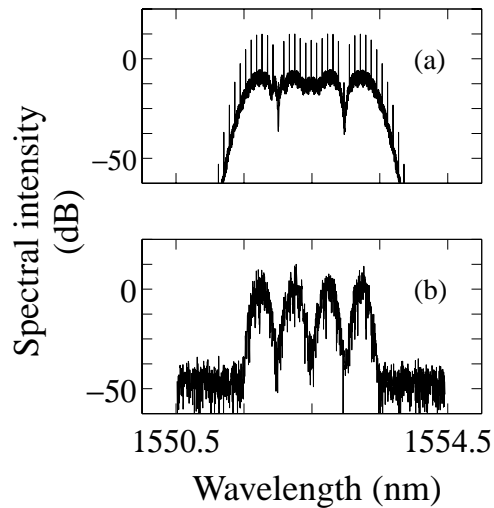


Figure 5.11: The evolution of the spectrum, while (a) corresponds to the input and (b) shows the output after 10,000 km propagation.

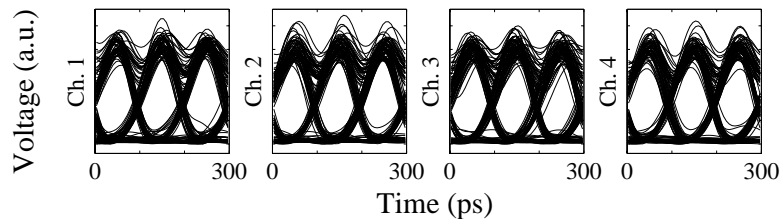


Figure 5.12: The output eye diagrams of all the channels in the system.

The sources of the errors come from the signal-spontaneous beat noise led by the pulses interaction as seen in Fig. 5.12 as well as the timing jitter mostly due to collisions shown in Fig. 5.13. The timing jitter in the single channel case is less than 2 ps. Figures 5.14 show the estimation of Q -values using 100 Monte Carlo realizations.

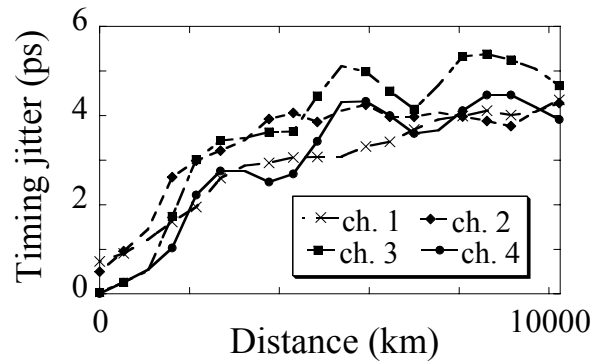


Figure 5.13: Timing jitter as a function of distance in the system.

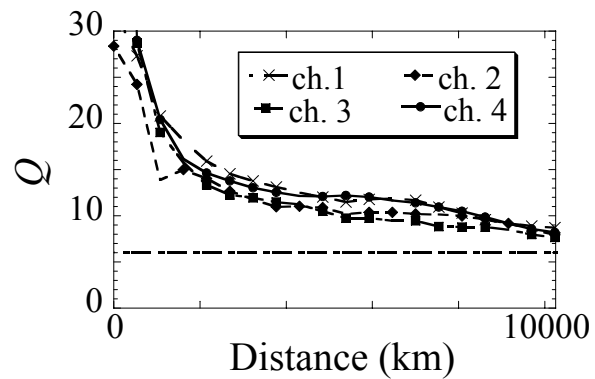


Figure 5.14: The Q -values as a function of distance in the system. The lower dashed line represents $Q = 6$ corresponding to a $\text{BER} \leq 10^{-9}$.

These results indicate that the error free distance of this WDM system could be over 10,000 km.

Chapter 6

Convergence of the Tyco-CRZ, CNET-DMS, and KDD-RZ WDM systems

6.1 Introduction

There has been a long debate in the optical communications community as to whether a soliton modulation format or a non-soliton modulation format such as non-return-to-zero is preferable for high-data-rate wavelength division multiplexed communications. Over the last decade, as individual channel data rates and the number of WDM channels have continued to grow, both formats have evolved substantially. Solitons have evolved into dispersion managed solitons, and NRZ has evolved into chirped return-to-zero. There are a number of successful laboratory testbed WDM systems that have been experimentally demonstrated. Among them is the system of Bergano, *et al.* at Tyco [1], [2], referred to by the authors as a CRZ system, that models a transoceanic link. Also among them is the system of Favre, *et al.* [3] and Le Guen, *et al.* [4], [5]

at CNET, referred by the authors as a DMS system, that models a terrestrial link. Among them as well is the system of Taga, *et al.* [6]–[8] at KDD, referred to as a return-to-zero (RZ) system, that models a transoceanic link. These experimental systems have been described in recent OFC postdeadline sessions [1], [2], [4]–[6], articles in *Electronics Letters* [3], [7], and an article in the *Journal of Quantum Electronics* [8]. So, in some sense they represent the state of the experimental art, at the time they were presented, for laboratory demonstrations of high-data-rate WDM systems based on both soliton and non-soliton formats.

It is my and my colleagues' contention that the non-soliton and soliton formats have effectively converged. The result is a new format that some call CRZ, some call DMS, and others simply call RZ. My colleagues and I reached this conclusion by developing simulation models that resemble the Tyco-CRZ, CNET-DMS, and KDD-RZ systems and comparing the pulse evolution and characteristics in these systems. In all three systems, one begins with raised-cosine pulses that are produced by a LiNbO₃ modulator. One then chirps the input pulse. In the Tyco-CRZ and KDD-RZ systems, this chirp is imposed by a LiNbO₃ phase modulator. In the CNET-DMS system, this chirp is imposed by a 3.5-km length of dispersion-compensating fiber (DCF) *via* the Kerr effect. The pulses then evolve along the transmission line. All three systems use dispersion maps in which the pulse stretch and shrink substantially in one period. In addition to that, however, we find that the pulse duration at the end point of each map period changed substantially along the fiber at most wavelengths. At the end of the transmission, the pulse duration is substantially smaller in all three systems than at the beginning. We also found that the relationship between the initial pulse duration, the final pulse duration, the initial chirp, and the average dispersion in the transmission line is almost exactly predicted by linear theory. The

Kerr nonlinearity only plays a small role in the pulse evolutions at the powers at which pulses are transmitted in these three systems. This behavior contrasts strongly with the behavior in periodically-stationary DMS systems like the ones studied by Jacob, *et al.* [11] and Suzuki, *et al.* [55] in which the pulse returns to the same shape after every period in the dispersion map. Observation of the eye diagrams in all three systems shows that the noise-induced spread of the rails is dominated by spontaneous-signal beat noise, in contrast to the periodically stationary DMS systems, where the dominant noise effect is either timing jitter or exponentially-growing noise in the spaces. For these reasons, we refer to all three test systems as quasilinear.

By referring to these three systems as quasilinear, we do not intend to imply that nonlinearity is unimportant. Quite the contrary, nonlinearity plays a crucial role in all three systems, which are all designed to mitigate its effects. As one example, we may consider the Tyco-CRZ system. The dispersion in each of these channels is individually compensated. If nonlinearity was unimportant then it would not matter whether this compensation occurred at the beginning of the transmission, the end of transmission, or both. In fact, this system suffers the least impairment when the compensation is split almost exactly between the beginning and the end of the transmission [56], [57]. I will show later in this chapter that nonlinear inter-pulse intra-channel interactions can lead to substantial timing jitter, much like in standard soliton systems, unless the compensation is split between the beginning and the end [58]. While it is true as stated earlier that spontaneous-signal beat noise dominates the spread of the eye diagrams, it is also true that unless the nonlinearity is carefully mitigated there is a large contribution from nonlinear timing jitter.

In Sec. 6.2, I outline the system configurations. In Sec. 6.3, I describe the evolution of a single, typical channel. It is typical in the sense that the average dispersion in a

single period of the dispersion map is not unusually close to zero as would be required for the system to be periodically stationary. In Sec. 6.4, I present full WDM studies. Finally, Sec. 6.5 contains the conclusion.

6.2 Schematic configurations of the Tyco-CRZ, CNET-DMS, and KDD-RZ systems

Based on the experimental reports [1]–[9] as well as optimization in our own simulations, I developed simulation models that are intended to model as closely as feasible the three systems that I am studying.

In the Tyco-CRZ and KDD-RZ models, I used initial pulses with a raised-cosine shape driven by a sinusoidal voltage, and a cosinusoidal pulse modulation, described by the expressions:

$$q = \sqrt{\frac{q_0}{2} \{1 + \cos[B\pi \sin(\Omega t)]\}}, \quad (6.1)$$

$$\phi = A\pi \cos(\Omega t), \quad (6.2)$$

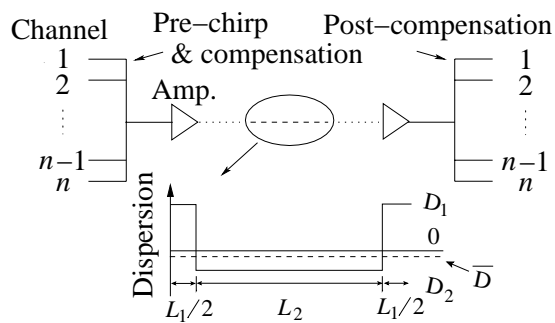
where in Eq. 6.1, the variable q_0 is the initial pulse intensity. The variable B is the modulation index of the voltage driver, and it can be adjusted to change the initial full width half maximum (FWHM) duration. In the Tyco-CRZ system, I set B equal to 1.0 corresponding to an initial input pulse with a FWHM duration of 32 ps, while in the KDD-RZ system, I chose $B = 0.7$ corresponding to an initial input pulse with a FWHM duration of 50 ps. In Eq. 6.2, the quantity A is the phase modulation depth, Ω is the bit rate of the signal, t is the time measured from the center of the bit window. The corresponding input chirp C is given by $C = \pi A\Omega^2$. In the simulation of CNET system, I launched the initial pulse shape described by Eq. 6.1, and I also

set B equal to 1 so that the initial pulse has a narrower FWHM pulse duration, which I verified is the optimal launching condition. I used a piece of DCF instead of a phase modulator to chirp the initial signal. The corresponding input chirp C is determined by solving Eq. 2.1 in the pre-chirping DCF, and then computing the negative of the second derivative of the phase at the center of the bit window.

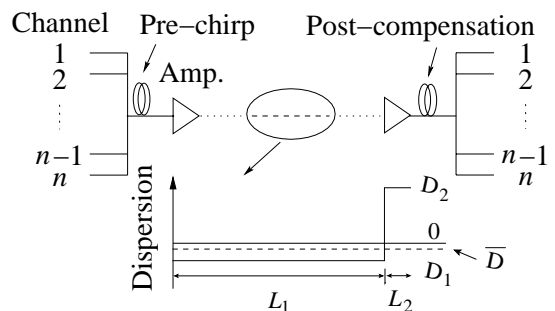
I show a schematic illustration of each of our three model systems in Fig. 6.1

A. Tyco-CRZ model

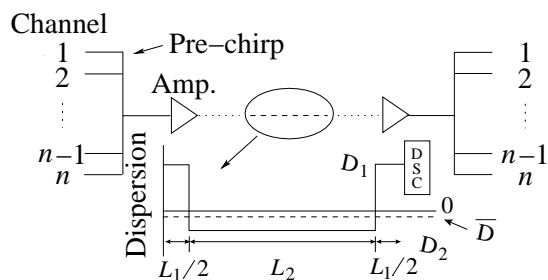
As shown in Fig. 6.1(a), the dispersion map that I used to study the Tyco-CRZ system has one segment of length $L_1 = 160$ km with $D_1 = -2.125$ ps/nm-km and a second segment of length $L_2 = 20$ km with $D_2 = 17$ ps/nm-km at 1550 nm, corresponding to the point at which the average dispersion over the map period is zero. The amplifier spacing is 45 km, and the total propagation distance is 5,040 km. For both types of fibers, I assume a dispersion slope $dD/d\lambda = 0.075$ ps/nm²-km as well as an effective area $A_{\text{eff}} = 50 \mu\text{m}^2$. The fiber loss is 0.21 dB/km, and the spontaneous emission factor $n_{\text{sp}} = 2.0$. These parameters correspond to the experiments of Bergano, *et al.* [1], [2], except that the dispersion map period is smaller. I chose a smaller period so that the dispersion management strength parameter γ_{map} corresponds to the value at which simulation studies showed the largest margin [59]. I chose a phase modulation depth $A = -0.6$ for the initial chirp and an average power of 0.3 mW per channel at the input, assuming an equal number of marks and spaces. I found that this choice of average power is nearly optimal [60]. I computed the average power by dividing the total optical energy over the entire computation time window. We compensate for the dispersion symmetrically, which, as noted earlier, is the optimal choice [58]. The path average pulse peak intensity \bar{P}_0 equals 0.24 mW



(a)



(b)



(c)

Figure 6.1: Schematic configuration of the three WDM model transmission systems: (a) Tyco-CRZ system, (b) CNET-DMS system, and (c) KDD-RZ system.

in this model system where $\gamma = 2.11 \times 10^{-3} \text{ m}^{-1}\text{W}^{-1}$. Hence the effective nonlinear length $L_{\text{NL,eff}} = 1/(\gamma P_0)$ in this system is about 1960 km so that $\gamma_{\text{NL}} = 2.6$. The minimum pulse duration at the end of the transmission is 21 ps in a channel that is offset -4.8 nm from the zero dispersion wavelength. For this channel, I find $\overline{D} = -0.36$ ps/nm-km, and I find a pulse spreading during transmission that is typical of most channels. We then find that dispersion length $L_{\text{D,eff}} = 960$ km, so that $\gamma_{\text{D}} = 5.3$.

B. CNET-DMS model

In my model of the CNET-DMS system, shown in Fig. 6.1(b), the map period is 120 km long and consists of a long span of standard single mode fiber (SMF) with a dispersion D_1 of 16.4 ps/nm-km at 1550 nm and a length L_1 of 102 km, followed by a shorter span of DCF with a dispersion D_2 of -95 ps/nm-km at 1550 nm and a length L_2 of 17.3 km. The dispersion slope of the SMF is 0.075 ps/nm²-km while the dispersion slope of the DCF is -0.2 ps/nm²-km so that it is possible to balance the dispersion and the dispersion slope of the SMF simultaneously. The A_{eff} of the SMF is $50 \mu\text{m}^2$ and a fiber loss is 0.2 dB/km, while A_{eff} equals to $20 \mu\text{m}^2$ with the fiber loss of 0.6 dB/km in DCF segment. The average dispersion \overline{D} is about 0.25 ps/nm-km with an average dispersion slope of 0.035 ps/nm²-km. In each period of the map, there is one amplifier following the SMF span and another one following the DCF span with $n_{\text{sp}} = 2.0$ in both amplifiers. The gain of the first amplifier $G_1 = 15.42$ dB, while the gain of the second amplifier $G_2 = 16.38$ dB, which minimizes the amplified spontaneous emission (ASE) noise accumulation during this dual-stage amplification. The total transmission distance is 1431.6 km. Since the dispersion slope is reduced by using DCF with a negative dispersion slope, the signals carried by all the wavelengths could be pre-chirped by propagation through a single 3.5-km-long

section of DCF (Pre-DCF) with a dispersion of -100 ps/nm-km at 1550 nm and the dispersion slope of -0.2 ps/nm²-km. The fiber loss is 0.5 dB/km with A_{eff} equal to 20 μm^2 . The residual average dispersion over the entire transmission line was adjusted by a piece of SMF fiber at the end of the transmission (Post-SMF) whose length was chosen to maximize the pulse compression at the end, leading to a residual average dispersion $\delta\bar{D}$ of approximately 0.034 ps/nm-km at the 1550 nm. This CNET-DMS model resembles the experimental system of Le Guen, *et al.* [5]. The typical average power in a WDM channel at the beginning of the transmission line is 1.2 mW. Just as in the Tyco-CRZ model, I numerically calculated the effective nonlinear length $L_{\text{NL,eff}} = 364$ km with $\bar{P}_0 = 1.3$ mW and the effective dispersion length $L_{\text{D,eff}} = 610$ km with $T_{\text{min}} = 14$ ps, so that $\gamma_{\text{NL}} = 3.9$ and $\gamma_{\text{D}} = 2.3$ respectively.

C. KDD-RZ model

The KDD-RZ model, shown in Fig. 6.1(c), contains a 1033-km-long dispersion shifted fiber (DSF) segment with $D_2 = -1.694$ ps/nm-km at 1550 nm. Before and after the DSF fiber segment, there is a segment of SMF with length $L_1/2$ of 50 km and a dispersion D_1 of 17.5 ps/nm-km at 1550 nm. Hence the path average dispersion is zero at 1550 nm. The average dispersion slope is 0.07 ps/nm-km in both the SMF and DSF segments. There are 20 amplifiers in the DSF segment equally spaced 51.65 km apart with $n_{\text{sp}} = 1.2$. I also placed amplifiers immediately after the segments of SMF that come before and after the DSF segment. My arrangement differs somewhat from the original KDD arrangement, in which the second SMF was put in the middle of the DSF span [6], [7]. I observed that one can achieve larger tolerance of the input pulse conditions, less oscillation of the pulse duration along the propagation, and a slightly larger dispersion compensation tolerance by choosing my arrangement. In

order to achieve an error-free WDM transmission over 9064 km, I used fibers with a large effective area $A_{\text{eff}} = 75 \mu\text{m}^2$ in both segments of the map. In an earlier study, my colleagues and I demonstrated that a fiber with a large effective area can significantly improve the eye degradation due to the nonlinear interactions [60]. The fiber loss is 0.21 dB/km. As in the Tyco-CRZ system shown in Fig. 6.1(a), there are individual phase modulators at the beginning of the transmission to pre-chirp the signal in each channel. Moreover, I also include a dispersion slope compensator (DSC) in each loop period, as what was done in the experimental demonstrations [6], [7]. The 23-rd amplifier was employed after the DSC module to compensate for the loss due to the DSC. Inside the DSC module, there are a pair of flat-top array waveguide gratings acting as a multiplexer (MUX) and demultiplexer (DEMUX) pair with a 3 dB bandwidth of 0.5 nm as well as a 1 dB bandwidth of 0.3 nm. The DEMUX separates channels before the individual dispersion compensation, and the MUX combines channels after the dispersion compensation. In the simulation, I include the effect of the array waveguide gratings by introducing a lumped filter. The filter function is

$$H(\omega) = \sqrt{H_0} \exp \left[-\frac{1}{2 \ln 2} \left(\frac{2\omega}{\omega_B} \right)^4 \right], \quad (6.3)$$

where the coefficient H_0 corresponds to the insertion loss, and ω_B corresponds to the 3 dB bandwidth. The loss of each array waveguide grating is 5 dB. Each individual channel has an independent dispersion compensation fiber of 5 km long followed by an erbium doped fiber amplifier (EDFA) to compensate for the loss of this dispersion compensation fiber and a 2 nm optical Gaussian filter to eliminate the ASE noise accumulation. The dispersion of the compensating fiber inside the DSC can be calculated individually according to the initial chirp. For a WDM channel that is offset by

-2.0 nm from the zero dispersion wavelength, I chose a residual average dispersion $\delta\bar{D} = -0.028$ ps/nm-km corresponding to the initial modulation depth $A = -0.4$. I set the unsaturated gain coefficient of the first 22 EDFAs $G_{1\dots 22,0}$ equal to 12.25 dB and the unsaturated gain of the last EDFA in the loop $G_{23,0}$ equal to 13 dB so that the average power in each WDM channel is about 0.44 mW. Consequently, the effective nonlinear length $L_{\text{NL,eff}} = 3140$ km with $\bar{P}_0 = 0.23$ mW and the nonlinear coefficient $\gamma = 1.4 \times 10^{-3} \text{ m}^{-1}\text{W}^{-1}$. The effective dispersion length L_{D} is 2290 km with $T_{\text{min}} = 24$ ps at the WDM channel we mentioned above. We thus obtain $\gamma_{\text{NL}} = 2.9$ and $\gamma_{\text{D}} = 4.0$.

I summarize the fiber parameters in all three systems in Table 6.1.

	fiber	D (ps/nm-km)	D' (ps/nm ² -km)	L (km)	A_{eff} (μm^2)	$n_2 \times 10^{-16}$ (cm ² /W)	α (dB/km)
(a)	SMF	17	0.075	20	50	2.6	0.21
	DSF	-2.125	0.075	160	50	2.6	0.21
(b)	SMF	16.4	0.075	102	50	2.6	0.21
	DCF	-95	-0.2	17.5	20	2.55	0.6
	Pre-DCF	-100	-0.2	3.5	20	2.55	0.5
	Post-SMF	16.4	0.075	2.9	50	2.6	0.21
(c)	SMF	17.5	0.07	100	75	2.55	0.21
	DSF	-1.694	0.07	1033	75	2.6	0.21

Table 6.1: The fiber parameters in three model WDM systems. (a) Tyco-CRZ system, (b) CNET-DMS system, and (c) KDD-RZ system.

Comparing the parameters of the three model systems, I find that the power in the CNET-DMS system is approximately 4 times larger than in the Tyco-CRZ system, but the total propagation length is approximately 3–4 times smaller. In the KDD-RZ system, (c) the power is about the same as in the Tyco-CRZ system; however, I used

a large effective area fiber that reduces the nonlinear coefficient by a factor of 1.5. Consequently, I found that the values of γ_{NL} are all within a factor of two of each other. The same is true for γ_{D} .

6.3 Intra-channel system behavior

I begin my study by focusing on the single-channel signal propagation, which allows us to explore a wider parameter space and to better understand the pulse evolution and characteristics in our three model systems. I will describe a case in which the average dispersion in the transmission line differs from zero by an amount which is typical for most channels in a WDM system and allows one to discuss the dynamics of the dispersion compensation. For the Tyco-CRZ system, I offset the channel wavelength from the zero dispersion point by -4.8 nm, while for the KDD-RZ system, I offset the channel wavelength from the zero dispersion point by -2.0 nm. For the CNET-DMS system, I do not offset the wavelength because the dispersion at the center wavelength already differs significantly from zero. Meanwhile, the better compensation of the third order dispersion implies that an offset is unnecessary. The compensation are using fibers. In the Tyco-CRZ and KDD-RZ cases, I fixed the length of fiber used for dispersion compensation as 10 km and 5 km respectively, but I varied the fiber dispersion to obtain the optimal average dispersion. I list the fiber parameters for the particular channels that I chose in the three model systems in Table 6.2.

I show the evolution of the FWHM of a single pulse at the end of each map period along the transmission line for each of our three model systems in Figs. 6.2–6.4. In each of these three model systems, the final pulse is compressed relative to the initial pulse by a factor of 1.5–2. However, the intermediate evolution is quite different in

	fiber	D (ps/nm-km)	β'' (ps ² /km)	\bar{D} (ps/nm-km)	$\bar{\beta}''$ (ps ² /km)	$\delta\bar{D}$ (ps/nm-km)	$\delta\bar{\beta}''$ (ps ² /km)	A
(a)	SMF	16.64	-21.33	-0.36	0.462	-0.028	0.036	-0.6
	DSF	-2.485	3.186					
(b)	SMF	16.4	-21.03	0.246	-0.315	0.034	-0.044	
	DSF	-95	121.79					
(c)	DSF	-1.824	2.351	-0.14	0.179	-0.028	0.036	-0.4
	SMF	17.36	-22.256					

Table 6.2: The fiber parameters in (a) Tyco-CRZ system, (b) CNET-DMS system, and (c) KDD-RZ system for a typical channel selected in the single channel studies.

all three cases. In the Tyco-CRZ system, shown in Fig. 6.2, the chirped pulse first stretches by 6–7 times its initial duration.

During the propagation, the residual average dispersion in the transmission, combined with the initial chirp, leads to a gradual pulse compression until the pulse

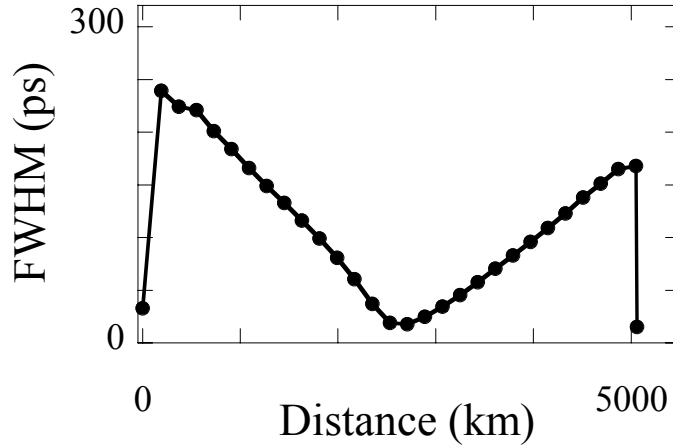


Figure 6.2: Evolution of the FWHM pulse duration at the end of each map period in the Tyco-CRZ system.

reaches its minimum duration at the midpoint of the propagation. Then, the pulse

stretches again until it resumes a pulse duration of 2-3 times the original duration before the final compression in the compensating fiber. I note that this gradual change in the pulse duration occurs in addition to the far more rapid change inside the dispersion map. The pulse expansion is large in the Tyco-CRZ system because

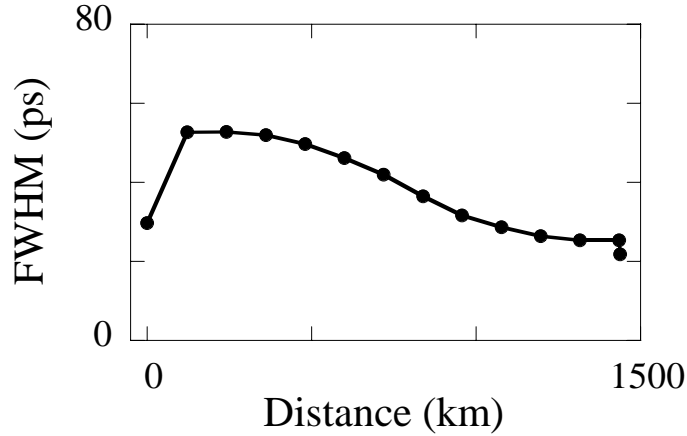


Figure 6.3: Evolution of the FWHM pulse duration at the end of each map period in the CNET-DMS system.

the compensation is only done at the beginning and the end of the transmission line. By contrast, the CNET-DMS system uses in-line DCFs that nearly compensate both the dispersion and the dispersion slope in every map period along the line, although the remaining dispersion is still sizeable, which minimizes inter-channel interactions. The initial stretch is produced by dispersion in the pre-chirp DCF. Moreover, the chirp that is produced by the pre-chirp DCF fiber is smaller than what is produced by phase modulation. The pulses only stretch a little under twice their initial pulse duration and then gradually compress during the remaining propagation to their final pulse duration shown in Fig. 6.3. In the KDD-RZ system seen in Fig. 6.4, the dispersion is compressed every 1000-km-long loop period.

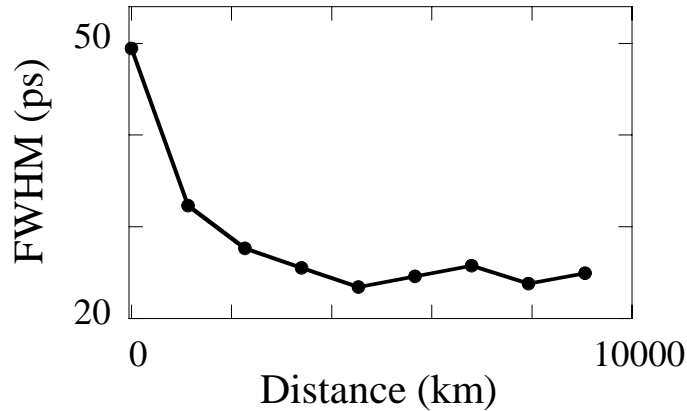


Figure 6.4: Evolution of the FWHM pulse duration at the end of each map period in the KDD-RZ system.

In this case, the pulse compresses continually during its propagation through the system with most of the compression occurring in the first couple of periods of the dispersion map. Imperfect compression along with a residual chirp leads to small oscillations in the pulse duration at the end of the pulse propagation.

Despite the large differences in the evolution of the three model systems, there is one important similarity that is clearly visible. All three systems use an initial chirp, in combination with the residual average dispersion, to compress the pulse at the end. One can better understand the pulse compression by comparing the observed behavior to the linear propagation of a Gaussian-shape pulse [60]. This theory developed by my colleagues and I predicts that the output pulse duration T_{out} at a distance $z = Z$ is related to the input pulse duration T_{in} through the relation

$$\frac{T_{\text{out}}}{T_{\text{in}}} = \left[\left(1 + \frac{c_0 \delta \bar{\beta}'' Z}{T_{\text{in}}^2} \right)^2 + \left(\frac{\delta \bar{\beta}'' Z}{T_{\text{in}}^2} \right)^2 \right]^{1/2}. \quad (6.4)$$

where we let $c_0 = CT_{\text{in}}^2 = \pi A \Omega^2 T_{\text{in}}^2$, where I recall C is the chirp parameter, A is the modulation depth, $\Omega/2\pi$ is the bit rate, and $\delta \bar{\beta}''$ is the residual average dispersion.

One can see that when $\delta\bar{\beta}''c_0 < 0$, the pulse will initially compress. In this case the minimal pulse duration T_{\min} occurs at $Z = Z_{\min}$, and their values are given by

$$Z_{\min}\delta\bar{\beta}'' = -\frac{c_0}{1+c_0^2}T_{\text{in}}^2, \quad (6.5)$$

$$\frac{T_{\min}}{T_{\text{in}}} = \frac{1}{(1+c_0^2)^{1/2}}. \quad (6.6)$$

I have compared the predictions of this simple linear theory to the optimized evolution in our three model systems. I have also compared a modified linear theory in which I solve the propagation equation Eq. 2.1, with the same initial conditions as in the complete theory, but with the Kerr nonlinearity turned off. We show the results of this comparison in Fig. 6.5 for the Tyco-CRZ and CNET-DMS systems. I see that the Gaussian approximation is qualitatively useful, but it is not quantitatively exact. By contrast the modified linear theory predicts output pulse durations for the Tyco-CRZ model system that agree with the prediction of the full nonlinear theory within 10% to 15%. In the CNET-DMS model system, the pulses are less chirped; so, the discrepancies are somewhat larger. I have not included the KDD-RZ system in Fig. 6.5 because stable pulses only exist for a limited range of the chirp parameters $-5.2 \text{ GHz/ps} < C < -3.7 \text{ GHz/ps}$. Within this range, the residual average dispersion $\delta\bar{D}$ only varies between -0.03 ps/nm-km to -0.02 ps/nm-km correspondingly, and the ratio $T_{\text{out}}/T_{\text{in}}$ varies between 0.53 and 0.67. These ranges are limited by the strong filtering that occurs due to cascading the narrow band MUX and DEMUX elements in the DSCs. I found that when $A = -0.4$, corresponding to $C = -4.96 \text{ GHz/ps}$, the values of $\delta\bar{D}$ and the ratio of $T_{\text{out}}/T_{\text{in}}$ predicted by the full nonlinear model are -0.028 ps/nm-km and 0.53, by the modified linear model are -0.023 ps/nm-km and 0.51, by the Gaussian model are -0.038 ps/nm-km and 0.2. The discrepancy between

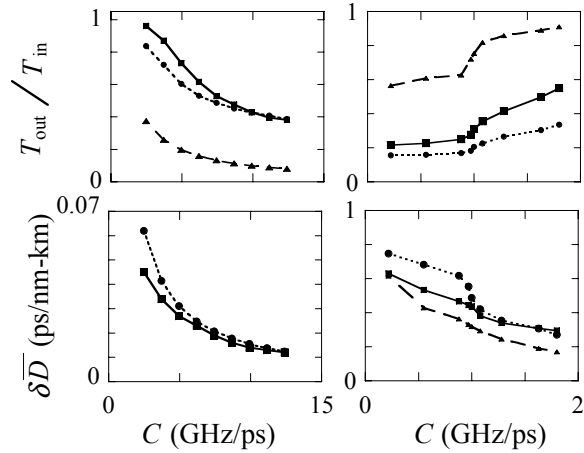


Figure 6.5: Dependence on the chirp C of (a) the final pulse compression and (b) the optimal residual average dispersion in Tyco-CRZ and CNET-DMS systems. The short-dashed lines with filled circles are the results predicted by modified linear theory, the solid lines with squares represent the result of full nonlinear model, while the long-dashed lines with triangles represent to the prediction from Gaussian theory. The left side corresponds to the results in Tyco-CRZ system while the right side represents the results in CNET-DMS system. I do not show Gaussian theory in the dependence of the chirp vs. the optimal residual average dispersion in the Tyco-CRZ system (the left lower figure) since there is no visible difference between the Gaussian theory and the modified linear theory.

the full nonlinear theory and the modified linear theory is only 20%.

These pulse evolution differ significantly from the evolution of periodically-stationary, dispersion-managed solitons. Their maximum stretching factors must be less than a factor of about 3 to avoid large nonlinear impairments [33]. The large stretching factor leads to a smaller path average peak power and hence a longer nonlinear scale length, as I discussed in Sec. 6.2, resulting in a significant reduction in the effect of nonlinearity. Figures 6.6–6.8 show the pulse shape inside one selected map period.

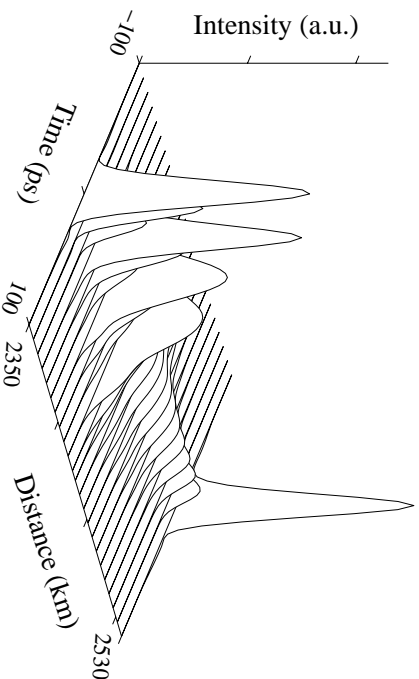


Figure 6.6: Evolution of the pulse shape inside one map period in the mid-way in the Tyco-CRZ system

In general, I notice that the ratios of the maximum to the minimum pulse duration in those systems are never larger than a factor of 2–3.

I now turn from an examination of single pulse propagation to examination of a complete channel consisting of a 64 bit pseudo-random bit stream. Using the same parameters as in Figs. 6.2–6.4, I show the electrical eye diagrams for all three systems in Figs. 6.9–6.11. In order to determine the principal source of the impairments, I sequentially turn off (a) both the ASE noise and the nonlinearity, (b) just the ASE noise, (c) just the nonlinearity, and (d) neither. In the case of the Tyco-CRZ system

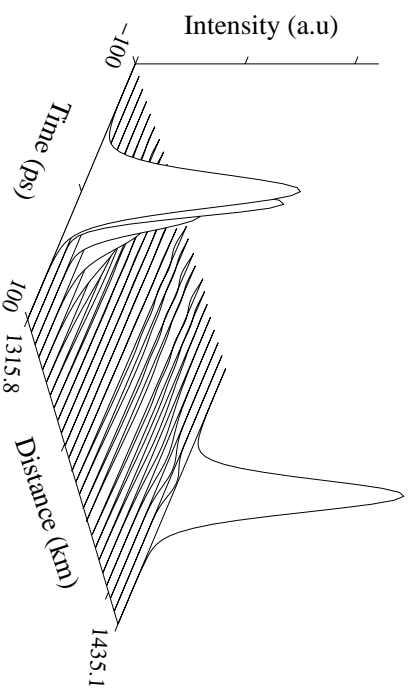


Figure 6.7: Evolution of the pulse shape inside the last map period in the CNET-DMS system

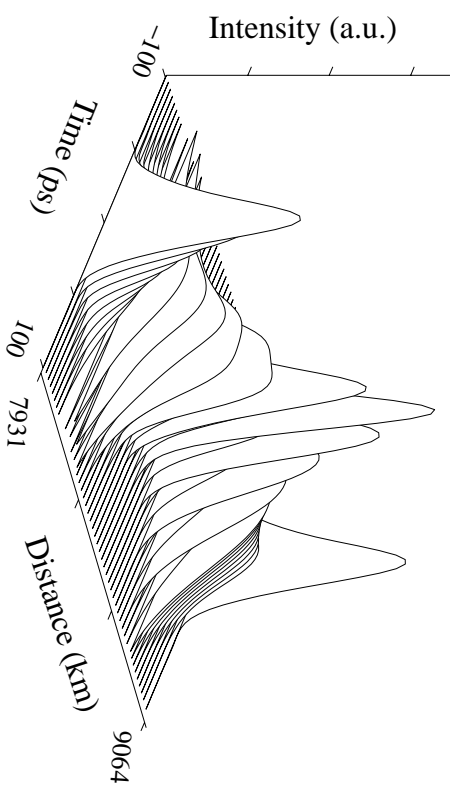


Figure 6.8: Evolution of the pulse shape inside the last map period in the KDD-RZ system

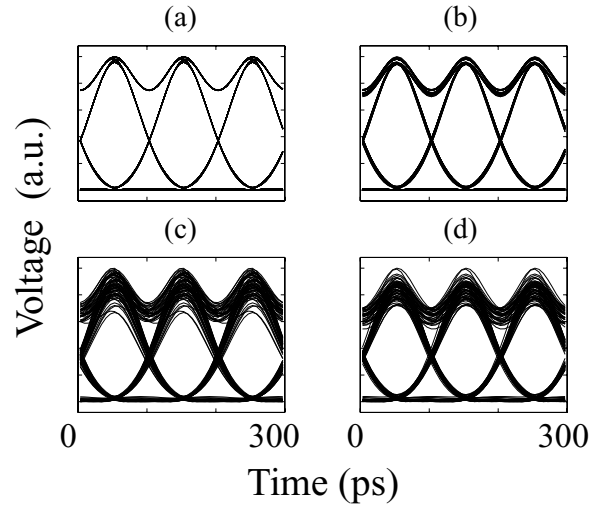


Figure 6.9: Eye diagrams in a single channel case in the Tyco-CRZ system, where (a) shows the case in which neither nonlinearity nor ASE noise is included in Eq. 2.1, (b) shows the case where we only neglect the ASE noise, (c) shows the case where I only neglect the nonlinearity in the simulations, and (d) shows the case where neither nonlinearity nor ASE is neglected.

and the CNET-DMS systems, the spontaneous-signal beat noise clearly dominates the impairments. In the case of the KDD-RZ system, nonlinearity does strongly impact the eye diagrams. However, the impairments in the center of the bit window, where the detection takes place, is dominated by signal-spontaneous beat noise.

As I mentioned earlier nonlinearity plays an important role in all three model systems. A good example is in the Tyco-CRZ system, in which I found that unless dispersion compensation is divided between the beginning and the end of the transmission, the eye diagrams exhibit substantial timing jitter [58].

Keeping the overall system parameters the same, I examined three dispersion

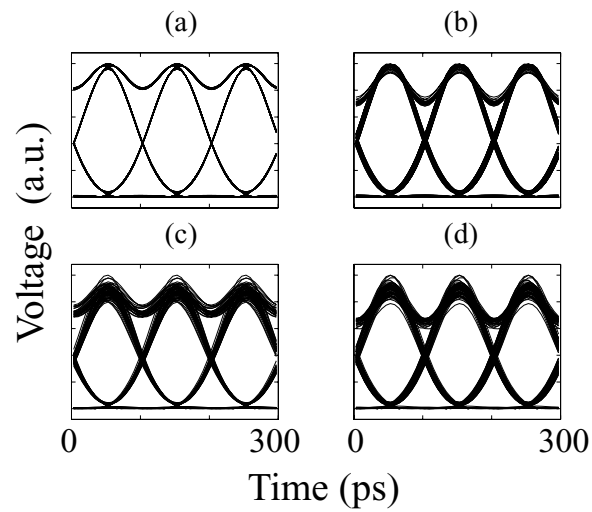


Figure 6.10: Eye diagrams in a single channel case in the CNET-DMS system, where (a)–(d) are the same as in Fig. 6.9.

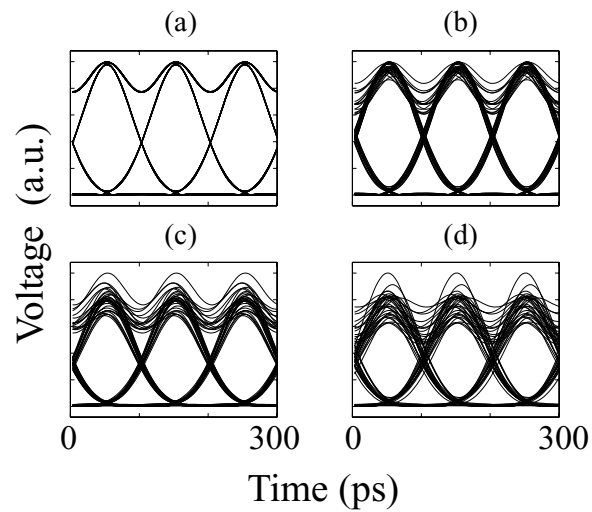


Figure 6.11: Eye diagrams in a single channel case in the KDD-RZ system, where (a)–(d) are the same as in Fig. 6.9.

slope compensation schemes for the channel I used previously in Tyco-CRZ system, (1) pre-compensation—only adding the dispersion compensation at the beginning, (2) post-compensation—only adding the compensation at the end, and (3) symmetric compensation—adding equal amounts of compensation at the beginning and at the end.

Figure 6.12 shows the input and outputs of a 64-bit pulse train that went through the transmission link in all three configurations. Figs. 6.12(c) and (d) suggest that

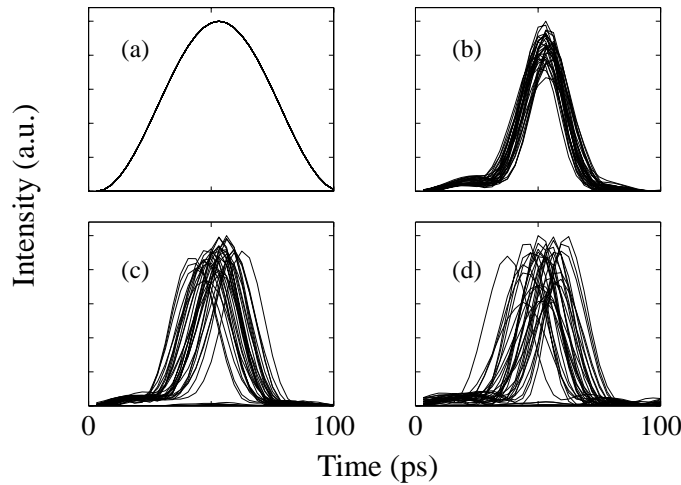


Figure 6.12: Optical eyes before and after the transmission line in a single channel study in Tyco-CRZ system. I show (a) the input and (b)–(d) the output with (b) symmetric compensation, (c) pre-compensation, and (d) post-compensation.

most of the degradation from asymmetric compensation is due to nonlinearly-induced timing jitter from inter-pulse interactions.

In order to explore the physical reason why symmetric slope compensation reduces the intersymbol interference due to nonlinearly-induced timing jitter, I considered a

case in which I only launched two pulses, separating by 100 ps. Using the definitions

$$\langle t \rangle = \frac{\int t |q(t)|^2 dt}{\int |q(t)|^2 dt} \quad \text{and} \quad \langle f \rangle = \frac{\int f |\tilde{q}(f)|^2 df}{\int |\tilde{q}(f)|^2 df}, \quad (6.7)$$

we carefully traced the pulse positions along the transmission link, then we calculated the offsets of the pulse positions in the time and frequency domains separately according to:

$$\Delta t = \langle t \rangle - t_0 \quad \text{and} \quad \Delta f = \langle f \rangle - f_0, \quad (6.8)$$

where $q(t)$ and $\tilde{q}(f)$ are the pulse profiles in the time and frequency domains respectively, and t_0 and f_0 are the initial positions of the pulses. I calculated the pulse positions at the end of each map, and, in order to retrieve the individual pulse shapes in the middle of the transmission link, I added a dispersive correction each time I detected the pulses, whose size was calculated by setting the total dispersion after the dispersive correction to optimally balance the initial chirp so that the pulses are maximally compressed. I found the results shown in Fig. 6.13. For each of the three cases, I also show $\Delta = \int_0^Z D(z') dz'$, the total dispersion accumulation, where Z is the propagation distance along the optical fiber. I note that there is a substantial frequency shift in all three compensation schemes. There is a tendency for the pulses to initially attract due to nonlinearity, just as in the case of solitons, and the pulses must shift their frequencies in opposite directions to attract. This frequency shift, followed by the motion of the pulses towards each other, leads to timing jitter. However, in the case of symmetric compensation, the dispersion reverses its sign midway through the transmission. As a consequence, two pulses that initially attracted each other begin to repel, and the effect is for the motion in the second half of the transmission to nearly erase the motion in the first half of the transmission.

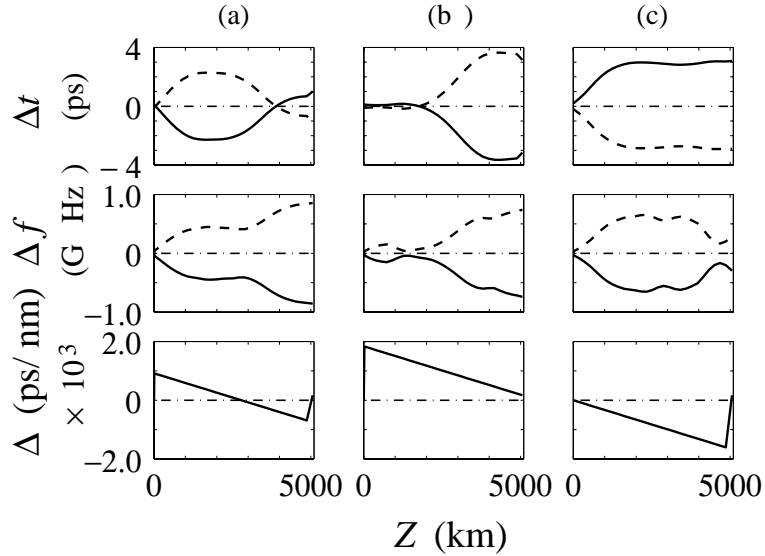


Figure 6.13: The offset of the CRZ pulse pairs in the time and frequency domains, as well as the accumulated dispersion in the individual configurations: (a) symmetric compensation, (b) pre-compensation, and (c) post-compensation. The dashed line corresponds to the earlier pulse, and the solid line corresponds to the later pulse.

These results have important implications for system design. Dispersion compensation is commonly used in most systems with single channel data rates at 10 Gb/s, and there is typically a substantial overlap between neighboring pulses in any 10 Gb/s system, whether it is based on an RZ or an NRZ format. (In the latter case, the pulses may consist of several bits.) The nonlinear pulse attraction results in timing jitter, particularly of isolated marks in an NRZ system. However, by carefully designing the dispersion map to be nearly symmetric, it is possible to minimize this effect.

I conclude that in all three model systems, the behavior resembles linear system in two important respects. First, the pulse dynamics is dominated by the linear

dispersion and the initial chirp. The nonlinearity plays a relatively small role in the single pulse dynamics. Second, signal-spontaneous beat noise dominates the growth of impairments in the electrical eye diagrams. This behavior is typically for linear systems. At the same time nonlinearity plays an important role in all three model systems. In particular, as mentioned earlier, I have shown that unless dispersion compensation is divided between the beginning and the end of the transmission in the Tyco-CRZ system, the eye diagrams exhibit substantial timing jitter [58]. In other words, a property that is typical of linear system—that the spread in the eye diagrams is dominated by spontaneous-signal beat noise—does not hold unless the nonlinearity is properly mitigated! Thus, we refer to these systems as quasilinear to indicate that they behave as if they were linear in important respects, but that nonlinearity and its mitigation play important roles.

6.4 WDM studies

In this section, I will study the performance of our three model systems with WDM. I keep 7 or 8 channels in our studies, which previous work indicates is sufficient to study the channel interactions in a full WDM system [61]. Channels that are far away do not affect each other much because they pass through each other quickly due to dispersion. In the WDM systems that I modeled, the channels are evenly spaced in wavelength, and each wavelength has a slightly different average dispersion. In all my WDM simulations, I assumed that the EDFA has the same gain for all the WDM channels. In reality, an accumulated gain difference must be avoided by using passive, gain-equalizing filters [51], [62], .

Comparing the results of this section to those of the previous sections allows us

to determine the importance of the inter-channel interference and to verify that the pulse behaviors that I observed in my single-channel studies are not significantly altered by inter-channel interactions. I kept 7 channels in the studies of the Tyco-CRZ and CNET-DMS systems, and I kept 8 channels in my studies of the KDD-RZ system. I used the same system parameters as in Sec. 6.3. The channel spacing in the Tyco-CRZ and CNET-DMS systems is 0.6 nm, while in the KDD-RZ system it is 0.8 nm. In the Tyco-CRZ system I placed channel 4 at the zero average dispersion wavelength, which is 1550 nm; in the CNET-DMS system, I placed channel 4 at 1550 nm; however, the corresponding dispersion significantly deviates from zero. In the KDD-RZ system, I place channels symmetrically around the central wavelength of 1550 nm, and the zero dispersion occurs in between channels 4 and 5. The channel spacing in the Tyco-CRZ model system is larger than in the experimental systems, but I did not use orthogonal polarizations in neighboring channels or forward error correction coding. In the CNET-DMS model system, I use a bit rate of 10 Gbit/s instead of 20 Gbit/s, but I did not use orthogonal polarizations in neighboring bits to generate a 20 Gbit/s pulse trains. I applied the same pre-chirping and the same residual average dispersion for all 7 channels in the Tyco-CRZ system. I fixed the length of the pre- and post-compensation fibers at 10 km for all 7 channels, but I varied the fiber dispersion to obtain the optimal average dispersion. In the experimental system, one must vary both the fiber type and the length to obtain optimal average dispersion. However, I have verified that as long as the accumulated dispersion in the pre- and post-compensation fibers are correct, the result does not change. In the CNET-DMS system, there is no individual pre-chirp and post-compensation for each channel. Since the dispersion slope is small at the end of each map period, it is possible to use one piece of fiber to pre-chirp the pulse in all the channels, and, at

the end, to use one post-compensation fiber to recover the pulse in all the channels. In the KDD-RZ system, I used the same chirp for all 8 channels, but the residual average dispersion after one loop period differs slightly from channel to channel, as shown in Table 6.3. I fixed the length of compensating fiber at 5 km but varied the fiber dispersion to obtain the optimal residual average dispersion.

Ch.	A	$\delta\overline{D}$ (ps/nm-km)	$\delta\overline{\beta}''$ (ps ² /km)
1	-0.4	-0.033	0.042
2	-0.4	-0.028	0.036
3	-0.4	-0.024	0.031
4	-0.4	-0.020	0.026
5	-0.4	-0.023	0.029
6	-0.4	-0.018	0.023
7	-0.4	-0.013	0.017
8	-0.4	-0.018	0.023

Table 6.3: The residual average dispersion in the 8 WDM channels of the KDD-RZ system, where Ch. = channel.

The simulation results for the input and output spectra are shown in Figs. 6.14-6.16. There is a tendency for the spectral intensity to decrease in between the channels in the KDD-RZ transmission system due to the cascading of the DSC, which includes a MUX and DEMUX pair that gradually narrows the signal spectrum. In Figs. 6.17-6.19, I showed the eye diagrams at the receivers in these systems. The eye diagrams are similar to what were obtained in the single channel system but with more amplitude jitter.

In the case of the Tyco-CRZ system, I observe somewhat more degradation in channel 4 than in channel 2 or in channel 6. This increased degradation in channel 4 is due to low average dispersion in every single map period along the line, which

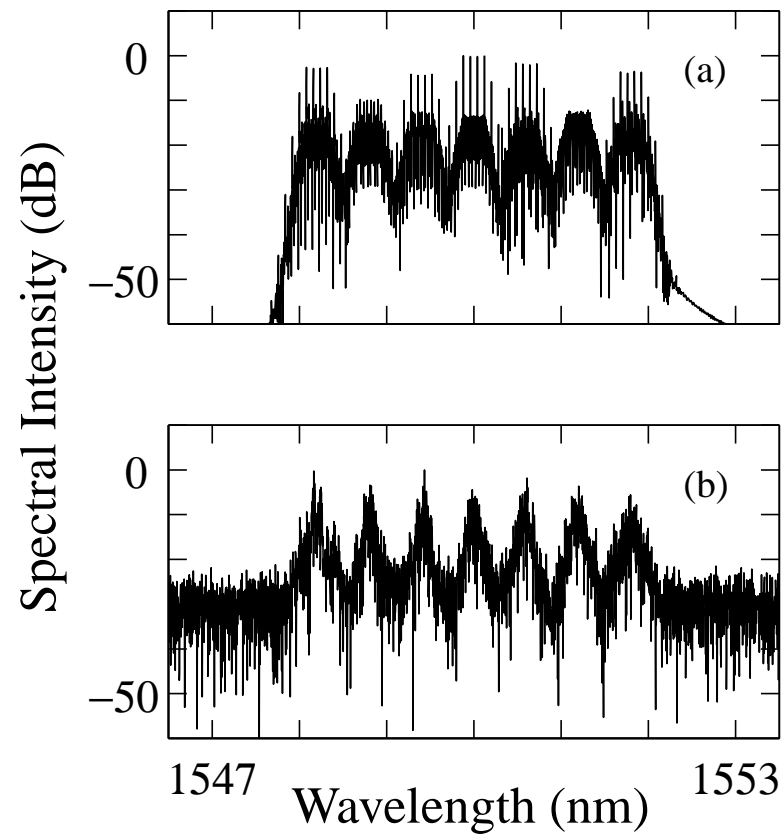


Figure 6.14: Evolution of the (a) input and (b) output spectral intensity in the Tyco-CRZ system.

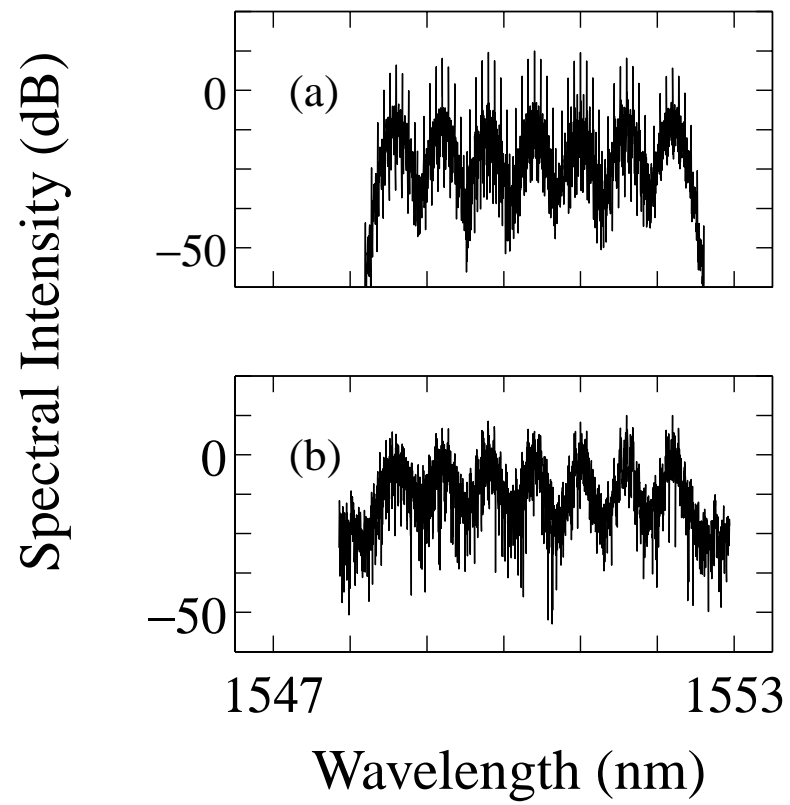


Figure 6.15: Evolution of the (a) input and (b) output spectral intensity in the CNET-DMS system.

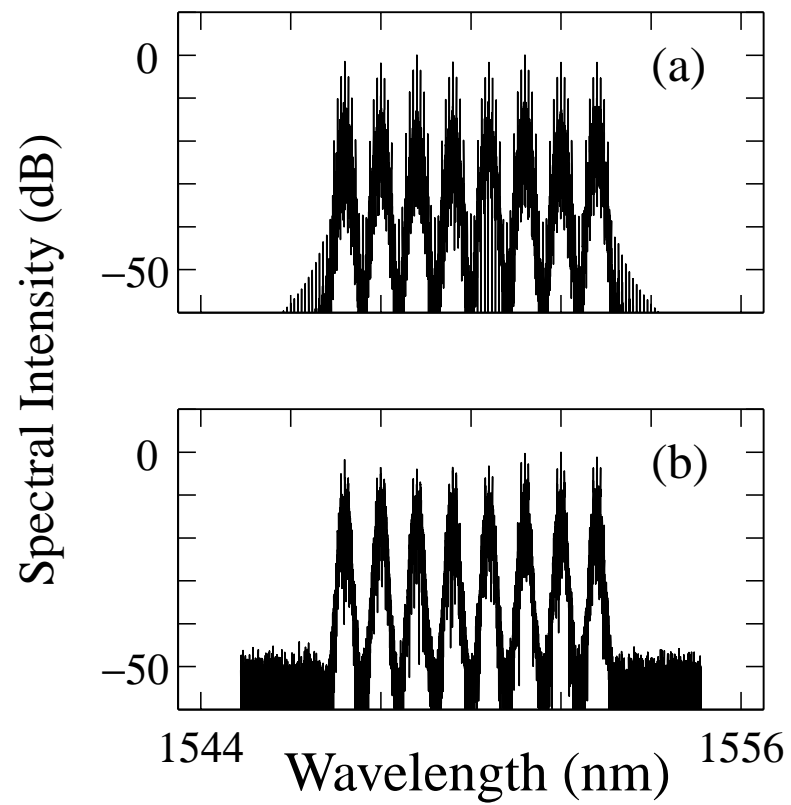


Figure 6.16: Evolution of the (a) input and (b) output spectral intensity in the KDD-RZ system.

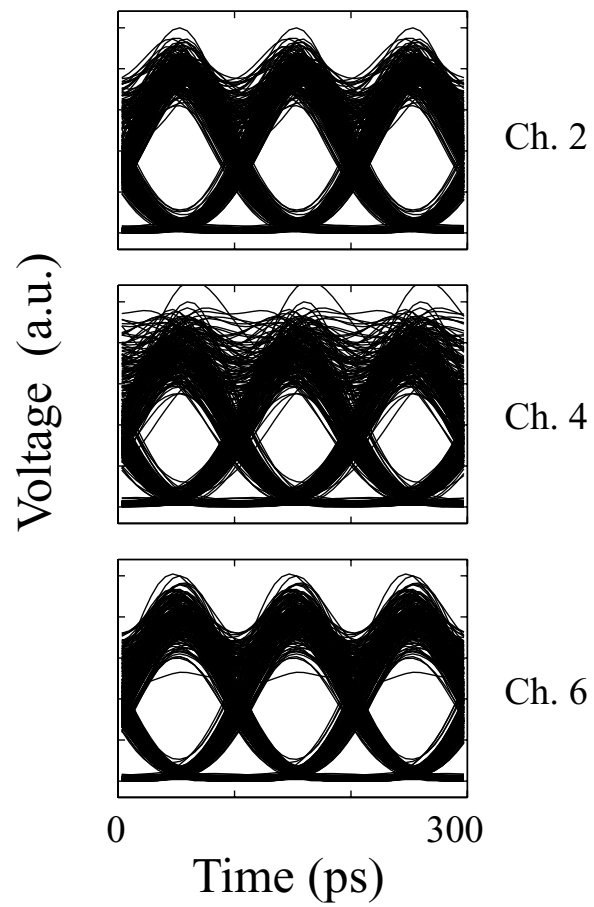


Figure 6.17: Eye diagrams of three channels in the 7×10 Gbit/s Tyco-CRZ WDM system.

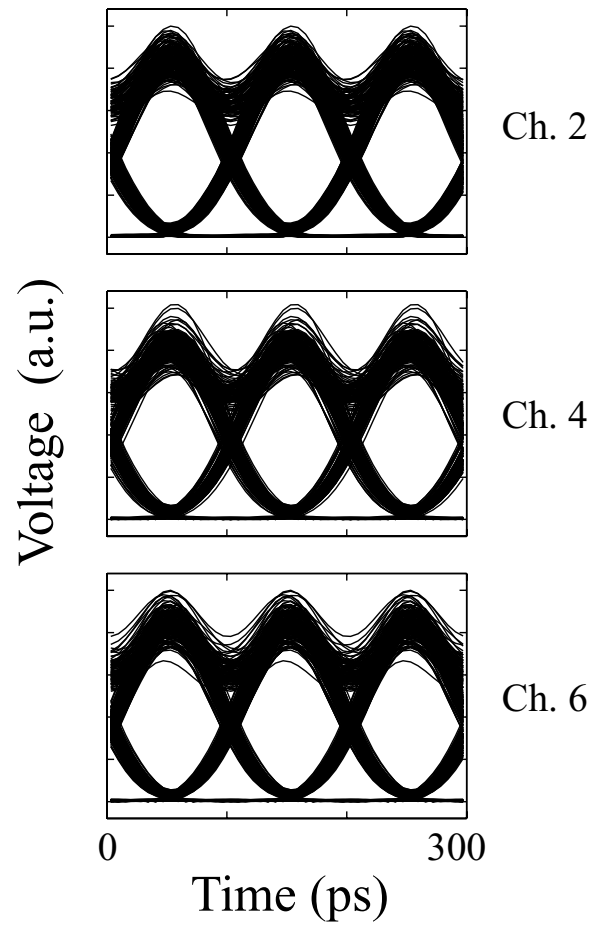


Figure 6.18: Eye diagrams of three channels in the 7×10 Gbit/s CNET-DMS WDM system.

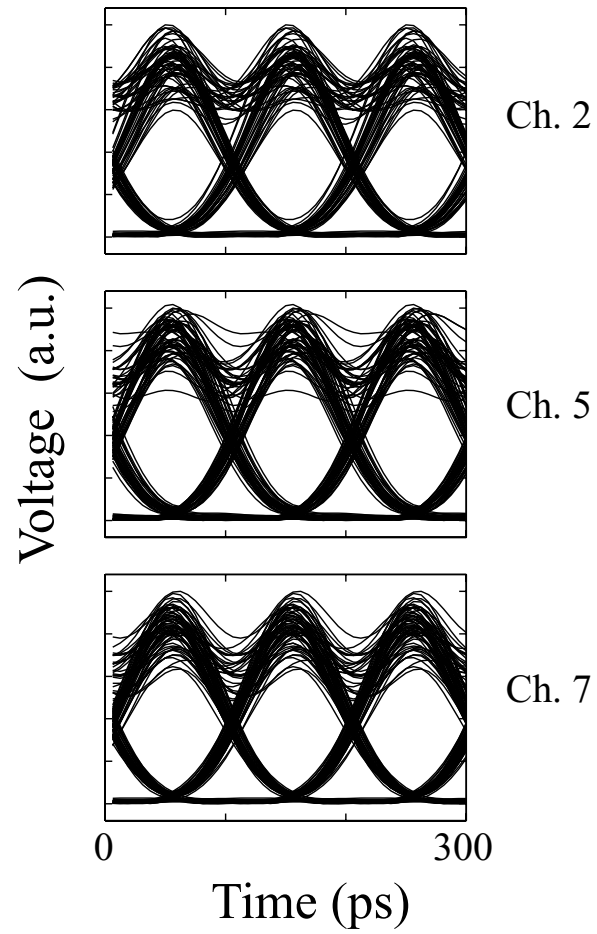


Figure 6.19: Eye diagrams of three channels in the 8×10 Gbit/s KDD-RZ WDM system.

increases the nonlinear inter-channel interactions.

While I do not show detailed plots of the pulse dynamics here, I have verified that the pulse dynamics is not visibly changed by the inter-channel interactions.

I conclude that wavelength division multiplexing degrades the eye diagrams in our three model systems, but it does not change their quasilinear behavior.

6.5 Conclusion

There has been a long debate in the optical fiber communications community over whether it would be preferable to use an NRZ format or a soliton format in long-haul systems. In recent years, the NRZ format has evolved into the CRZ format, while the soliton format evolved into the periodically-stationary DMS format and from there into the non-periodically stationary or quasilinear DMS format. It is our view that the soliton and non-soliton formats have effectively converged.

In this portion of my studies, I compared three systems that exemplify modern-day CRZ, DMS, and RZ systems. I did so by creating computer models that reproduce the essential features of all three systems as closely as feasible. I found that the pulse dynamics is dominated by the initial chirp of the pulses and the linear dispersion in the transmission line. I also found that the spread in the electronic eye diagrams is dominated by spontaneous-signal beat noise. This behavior is typical for linear systems. At the same time, I also found that nonlinearity plays an important role in all three systems and must be properly mitigated in order for the typically linear behavior that I just mentioned to manifest itself. We refer to these systems as quasilinear to indicate that the pulse dynamics and eye diagrams in these systems resemble those in linear systems, while the nonlinearity plays an important role. These systems resemble

each other far more closely than any of them resembles the periodically-stationary DMS systems of Jacob, *et al.* [11] or Sukuzi, *et al.* [55].

Chapter 7

Conclusion

We have come a long way in the 1990s toward determining a robust pulse format for higher bit rate signals, (over 10 Gbit/s) to carry densely wavelength division multiplexed digital information over trans-oceanic distances. Dispersion management revolutionized the traditional NRZ/soliton modulation formats. In this dissertation, I have explored various formats that are used in practice. I have concluded that the different formats have converged to a quasilinear format in WDM systems, whether they are labeled CRZ, DMS, RZ, or something else. While the details of the system designs may be quite different, there is no relationship between the design and the labels.

I began my investigation by presenting and validating the mathematical model that I used in comparison of the Tyco-CRZ, CNET-DMS, and KDD-RZ systems. I started the investigation by describing the modified NLS equations, ASE noise model, gain saturation models, and the method of estimating the system performance by examining the Q and timing jitter. Accumulation of ASE noise generated by EDFAs is known as the major source that dominates the degradation of the system performance. Physically, ASE noise can be regarded as a additive, white noise in the

fiber communication system. In order to properly estimate the system performance, it is necessary to use a correct ASE model in the system simulator. I validated the ASE model by studying timing jitter reduction in DMS systems. Solitons can propagate over long distances as a result of the balance of nonlinearity and dispersion, so that soliton-based systems are useful for validating models that are based on the solution of the nonlinear Schrödinger equation. In this set of studies present in Chap. 3, I carried out the calculation of Gordon-Haus jitter in a traditional soliton system to calibrate the simulator I built in the presence of ASE noise. The model gave a complete agreement with the analytical theory [16]. The model was also tested in DMS systems, and it yielded completely agreement with timing jitter calculations in DMS systems based on the semi-analytical approach developed by Dr. Grigoryan [17].

With the deployment of WDM technology in modern-day optical transmission systems, the optical power required to convey hundreds of channels naturally saturates in-line EDFAs. It is very important to consider the gain saturation effect in the study of WDM systems. This mechanism is also critical in a filtered DMS system or WDM systems with in-line filtering like. I carefully compared my numerical model to the experimental system that was built by Dr. Carter and his colleagues at the Laboratory for Physical Sciences, including the gain saturation model and the estimation of Q values. The results of comparison, shown in Chap. 4 indicate excellent agreement between simulation and experiment.

In Chap. 5, I studied a WDM design that could be used to extend the experiment at the Laboratory for Physical Sciences to WDM systems. This design was based on a 500 km loop with a dispersion slope compensating module that also compensation for gain variations. I showed that this design could produce a four-channel WDM DMS system in which error-free signal transmission could in principle occur over 10,000 km.

However, the allowed power margins were quite small, indicating that the practical interest of this system might be limited.

In Chap. 6, I compared three systems of current interest: the Tyco-CRZ system, the CNET-DMS system, and the KDD-RZ system. I demonstrated that all three systems operate in a quasilinear regime in which the pulse evolution is dominated by dispersion and the eye degradation is dominated by signal-spontaneous beat noise. At the same time, I demonstrate that nonlinearity plays an important role and its mitigation is critical. In particular, I show that symmetric compensation is required in the Tyco-CRZ system to avoid substantial timing jitter.

Bibliography

- [1] N. S. Bergano, C. R. Davidson, M. Ma, A. N. Pilipetskii, S. G. Evangelides, H. D. Kidorf, J. M. Darcie, E. A. Golovchenko, K. Rottwitt, P. C. Corbett, R. Menges, M. A. Mills, B. Pedersen, D. Peckham, A. A. Abramov, and A. M. Vengsarkar, “320 Gb/s WDM transmission (64×5 Gb/s) over 7,200 km using large mode fiber spans and chirped return-to-zero signals,” in *Proc. OFC'98*, (San Jose, CA), Feb. 1998, postdeadline paper PD12.
- [2] N. S. Bergano, C. R. Davidson, C. J. Chen, B. Pedersen, M. A. Mills, N. Ramanujam, A. B. Kidorf, H. D. Puc, M. D. Levonas, and H. Abdelkader, “640 Gb/s transmission of sixty-four 10 Gb/s WDM channels over 7,200 km with 0.33 (bits/s)/hz spectral efficiency,” in *Proc. OFC'99*, (San Diego, CA), Feb. 1999, postdeadline paper PD2.
- [3] F. Favre, D. Le Guen, M. L. Moulinard, M. Henry, and T. Georges, “320 Gbit/s soliton WDM transmission over 1300 km with 100 km dispersion-compensated spans of standard fiber,” *Electron. Lett.*, vol. 33, no. 25, pp. 2135–2136, 1997.
- [4] D. Le Guen, F. Favre, M. L. Moulinard, M. Henry, G. Michaud, L. Mac, F. Devaux, B. Charbonnier, and T. Georges, “200 GBit/s 100 km-span soliton WDM transmission over 1000 km of standard fiber with dispersion compensation and

- pre-chirping,” in *Proc. OFC'98*, (San Jose, CA), Feb. 1998, postdeadline paper PD17.
- [5] D. Le Guen, S. D. Burgo, M. L. Moulinard, D. Grot, M. Henry, F. Favre, and T. Georges, “Narrow band 1.02 Tbit/s (51×20 Gbit/s) soliton DWDM transmission over 1000 km of standard fiber with 100 km amplifier spans,” in *Proc. OFC'99*, (San Diego, CA), Feb. 1999, postdeadline paper PD4.
- [6] H. Taga, N. Edagawa, M. Suzuki, N. Takeda, K. Imai, S. Yamamoto, and S. Akiba, “213 Gbit/s (20×10.66 Gbit/s), over 9000 km transmission experiment using periodic dispersion slope compensator,” in *Proc. OFC'98*, (San Jose, CA), Feb. 1998, postdeadline paper PD13.
- [7] H. Taga, M. Suzuki, N. Edagawa, N. Takeda, K. Imai, S. Yamamoto, and S. Akiba, “20 WDM 10.66 Gbit/s transmission experiment over 9000 km using periodic dispersion slope compensation,” *Electron. Lett.*, vol. 34, no. 5, pp. 476–478, 1998.
- [8] H. Taga, M. Suzuki, N. Edagawa, S. Yamamoto, and S. Akiba, “Long-distance WDM transmission experiments using the dispersion slope compensator,” *J. Quantum Electron.*, vol. 34, no. 11, pp. 2055–2063, 1998.
- [9] T. Tsuritani, N. Takeda, A. Agata, I. Morita, H. Yamauchi, N. Edagawa, and M. Suzuki, “1 Tbit/s (100×10.7 Gbit/s) transoceanic transmission using 30 nm-wide broadband optical repeaters with A_{eff} -enlarged positive dispersion fiber and slope-compensation DCF,” in *Proc. ECOC'99*, (Nice, France), Oct. 1999, postdeadline paper PDII-8.

- [10] J. M. Jacob, E. A. Golovchenko, A. N. Pilipetskii, G. M. Carter, and C. R. Menyuk, "10 Gbit/s transmission of NRZ over 10,000 km and solitons over 13,500 km error-free in the same dispersion-managed system," *IEEE Photon. Technol. Lett.*, vol. 9, pp. 1412–1414, 1997.
- [11] J. M. Jacob and G. M. Carter, "Error-free transmission of dispersion-managed solitons at 10 Gbit/s over 24,500 km without frequency sliding," *Electron. Lett.*, vol. 33, pp. 1128–1129, 1997.
- [12] J. M. Jacob, E. A. Golovchenko, A. N. Pilipetskii, G. M. Carter, and C. R. Menyuk, "Experimental demonstration of soliton transmission over 28 mm using mostly normal dispersion fiber," *IEEE Photon. Technol. Lett.*, vol. 9, pp. 130–132, 1997.
- [13] G. M. Carter, J. M. Jacob, C. R. Menyuk, E. A. Golovchenko, and A. N. Pillipetskii, "Experimental evidence for timing jitter reduction for a dispersion-managed soliton system," *Optics Letters*, vol. 22, pp. 513–515, 1997.
- [14] G. M. Carter and J. M. Jacob, "Dynamics of solitons in filtered dispersion-managed systems," *IEEE Photon. Technol. Lett.*, vol. 10, pp. 546–548, 1998.
- [15] G. M. Carter, R.-M. Mu, V. Grigoryan, C. R. Menyuk, P. Sinha, T. F. Caruthers, M. L. Dennis, and I. N. Duling III, "Transmission of dispersion-managed solitons at 20 Gbit/s over 20,000 km," *Electronics Letters*, vol. 35, pp. 233–234, 1999.
- [16] J. P. Gordon and H. A. Haus, "Random walk of coherently amplified solitons in optical fiber transmission," *Opt. Lett.*, vol. 11, pp. 665–667, 1986.

- [17] V. S. Grigoryan, C. R. Menyuk, and R.-M. Mu, "Calculation of timing and amplitude jitter in dispersion-managed optical fiber communications using linearization," *J. Lightwave Technol.*, vol. 17, no. 8, pp. 1347–1356, 1999.
- [18] N. J. Smith, W. Forysiak, and N. J. Doran, "Reduced Gordon-Haus jitter due to enhanced power soliton in strongly dispersion managed systems," *Electron. Lett.*, vol. 32, no. 22, pp. 2085–2086, 1996.
- [19] H. Yoshimura, K. Sato, and N. Takachio, "10 Gbit/s soliton transmission over 2900 km using 1.3 μm singlemode fibers and dispersion compensation using chirped fiber bragg gratings," *IEEE Comm. Magazine*, vol. 35, no. 9, pp. 74–82, 1999.
- [20] P. Green, "Theoretical and experimental study of soliton transmission in dispersion managed links," *IEEE Comm. Magazine*, vol. E81, no. 2, p. 38, 1998.
- [21] T. Ito, K. Fukuchi, K. Sekiya, D. Ogasahara, R. Ohhira, and T. Ono, "6.4 Tb/s (160×40 GB/s) WDM transmission experiment with 0.8 Bit/s/Hz spectral efficiency," in *Proc. ECOC'00*, (Munich, Germany), Sept. 2000, postdeadline paper 1.1.
- [22] A. Färbert, G. Mohs, S. Spälter, J.-P. Elbers, C. Fürst, A. Schöpflin, E. Gottwald, C. Scheerer, and C. Glingener, "7 TB/s (176×40 GB/s) bidirectional interleaved transmission with 50 GHz channel spacing," in *Proc. ECOC'00*, (Munich, Germany), Sept. 2000, postdeadline paper 1.3.
- [23] S. Bigo, A. Bertaina, Y. Frignac, S. Borne, L. Lorcy, D. Hamoir, D. Bayart, J.-P. Hamaide, W. Idler, E. Lach, B. Franz, G. Veith, O. Sillard, L. Fleury, P. Guénot,

- and P. Nouchi, "5.12 TBit/s (128×40 GBit/s wdm) transmission over 3×100 km of Teralighttm fiber," in *Proc. ECOC'00*, (Munich, Germany), Sept. 2000, postdeadline paper 1.2.
- [24] C. R. Davidson, C. J. Chen, M. Nissov, A. Pilipetskii, N. Ramanujam, B. Kidorf, B. Pederson, M. A. Mills, C. Lin, M. I. Hayee, J. X. Cai, A. B. Puc, P. C. Corbett, R. Menges, H. Li, A. Elyamani, C. Rivers, and B. N., "1800 Gb/s transmission of one hundred and eighty 10 Gb/s WDM channels over 7,000 km using full EDFA C-band," in *Proc. OFC'00*, (Baltimore, MD), Mar. 2000, postdeadline paper PD25.
- [25] T. Naito, N. Shimojoh, T. Tanaka, H. Nakamoto, M. Doi, T. Ueki, and M. Suyama, "1 Tbit/s WDM transmission over 10,000 km," in *Proc. ECOC'99*, (Nice, France), Oct. 1999, postdeadline paper PDI-1.
- [26] K. Fukuchi, M. Kakui, A. Sasaki, T. Ito, Y. Inada, T. Tsuzaki, K. Shitomi, T. and Fujii, S. Shikii, H. Sugahara, and A. Hasegawa, "1.1-Tb (55×20 -Gb/s) dense WDM soliton transmission over 3,020-km widely dispersion-managed transmission line employing 1.55/1.58- μ m hybrid repeaters," in *Proc. ECOC'99*, (Nice, France), Oct. 1999, postdeadline paper PDII-4.
- [27] T. Tanaka, N. Shimojoh, T. Naito, H. Nakamoto, A. Suguyama, and M. Suyama, "2.1-TBit/s WDM transmission over 7,221 km with 80-km repeater spacing," in *Proc. ECOC'00*, (Munich, Germany), Sept. 2000, postdeadline paper 1.8.
- [28] N. S. Bergano, "Ultra long distance submarine DWDM systems," in *Proc. ECOC'00*, (Munich, Germany), pp. 67–68, Sept. 2000, paper 2.2.1.

- [29] G. P. Agrawal, *Nonlinear Fiber Optics*. Academic Press, 2nd ed., San Diego, CA, 1995.
- [30] I. Morita, M. Suzuki, N. Edagawa, K. Tanaka, S. Yamamoto, and S. Akiba, "Performance improvement by initial phase modulation in 20 Gbit/s soliton-based RZ transmission with periodic dispersion compensation," *Electron. Lett.*, vol. 33, no. 12, pp. 1021–1022, 1997.
- [31] N. J. Smith, F. M. Knox, N. J. Doran, K. J. Blow, and I. Bennion, "Enhanced power solitons in optical fibers with periodic dispersion management," *Electron. Lett.*, vol. 32, no. 1, pp. 54–55, 1996.
- [32] M. Matsumoto and H. A. Haus, "240-km repeater spacing in a 5280-km WDM system experiment using 8×2.5 Gb/s NRZ transmission," *IEEE Photon. Technol. Lett.*, vol. 9, no. 6, pp. 785–787, 1997.
- [33] T. Yu, E. A. Golovchenko, A. N. Pilipetskii, and C. R. Menyuk, "Dispersion-managed soliton interactions in optical fibers," *Opt. Lett.*, vol. 22, no. 11, pp. 723–725, 1997.
- [34] R.-M. Mu, T. Yu, V. S. Grigoryan, and C. R. Menyuk, "Convergence of the CRZ and DMS formats in WDM systems using dispersion management," in *Proc. OFC'00*, (Baltimore, MD), pp. 32–34, Mar. 2000, paper FC1.
- [35] R.-M. Mu, V. S. Grigoryan, C. R. Menyuk, G. M. Carter, and J. M. Jacob, "Comparison of theory and experiment for dispersion-managed solitons in a recirculating fiber loop," *IEEE J. Select. Topics Quantum Electron.*, vol. 6, no. 2, pp. 248–257, 2000.

- [36] C. R. Menyuk, “Application of multiple length scale methods to the study of optical fiber transmission,” *J. Eng. Math.*, vol. 36, no. 6, pp. 113–136, 1999.
- [37] R.-M. Mu, V. S. Grigoryan, C. R. Menyuk, E. A. Golovchenko, and A. N. Pilipetskii, “Timing jitter reduction in a dispersion-managed soliton system,” *Opt. Lett.*, vol. 23, no. 12, pp. 930–932, 1998.
- [38] T. Yu, R.-M. Mu, V. S. Grigoryan, and C. R. Menyuk, “Energy enhancement of dispersion-managed solitons in optical fiber transmission systems with lumped amplifiers,” *IEEE Photon. Technol. Lett.*, vol. 11, no. 1, pp. 75–77, 1999.
- [39] M. Matsumoto, “Theory of stretched-pulse transmission in dispersion-managed fibers,” *Opt. Lett.*, vol. 22, no. 16, pp. 1238–1240, 1997.
- [40] S. K. Turitsyn, “Theory of average pulse propagation in high-bit-rate optical transmission systems with strong dispersion management,” *JETP Lett.*, vol. 65, no. 11, pp. 845–851, 1997.
- [41] M. J. Ablowitz and G. Biondini, “Multiscale pulse dynamics in communication systems with strong dispersion management,” *Opt. Lett.*, vol. 23, no. 21, pp. 1668–1670, 1998.
- [42] D. Breuer, F. Küppers, A. Mattheus, E. G. Shapiro, I. Gabitov, and S. K. Turitsyn, “Symmetrical dispersion compensation for standard monomode-fiber-based communication systems with large amplifier spacing,” *Opt. Lett.*, vol. 22, no. 13, pp. 982–984, 1997.

- [43] S. Kumar, M. Wald, F. Lederer, and A. Hasegawa, "Soliton interaction in strongly dispersion-managed optical fibers," *Opt. Lett.*, vol. 23, no. 13, pp. 1019–1021, 1998.
- [44] Y. Kodama, S. Kumar, and A. Maruta, "Chirped nonlinear pulse propagation in a dispersion-compensated system," *Opt. Lett.*, vol. 22, no. 22, pp. 1689–1691, 1997.
- [45] M. Matsumoto, "Analysis of interaction between stretched pulses propagating in dispersion-managed fibers," *IEEE Photon. Technol. Lett.*, vol. 10, no. 3, pp. 373–375, 1998.
- [46] T.-S. Yang and W. L. Kath, "Analysis of enhanced-power solitons in dispersion-managed optical fibers," *Opt. Lett.*, vol. 22, no. 13, pp. 985–987, 1997.
- [47] E. G. Shapiro and S. K. Turitsyn, "Theory of guiding center breathing soliton propagation in optical communication systems with strong dispersion management," *Opt. Lett.*, vol. 22, no. 20, pp. 1544–1546, 1997.
- [48] V. S. Grigoryan, T. Yu, E. A. Golovchenko, C. R. Menyuk, and A. N. Pilipetskii, "Dispersion-managed soliton dynamics," *Opt. Lett.*, vol. 22, no. 21, pp. 1609–1611, 1997.
- [49] D. Marcuse, "Derivation of analytical expressions for the bit-error probability in lightwave systems with optical amplifiers," *J. of Lightwave Tech.*, vol. 8, pp. 1816–1823, 1990.
- [50] A. Mori, "Tellurite-based EDFAs for broadband communication," in *Proc. OFC'98*, (San Jose, CA), p. 97, Feb. 1998, paper WA1.

- [51] Y. Sun, J. W. Sulhoff, A. K. Srivastava, J. L. Zyskind, T. A. Strasser, J. R. Pedrazzini, C. Wolf, J. Zhou, J. B. Judkins, R. P. Espindola, and A. M. Vengsarkar, “80 nm ultra-wideband erbium-doped silica fibre amplifier,” *Electron. Lett.*, vol. 33, no. 23, pp. 1965–1967, 1997.
- [52] L. F. Mollenauer and P. V. Mamyshev, “Massive wavelength-division multiplexing with solitons,” *IEEE J. of Quantum Electron.*, vol. 34, no. 11, pp. 2089–2102, 1998.
- [53] L. F. Mollenauer, J. P. Gordon, and P. V. Mamyshev, *Optical fiber telecommunications III*, ch. 12. Academic, San Diego, CA, 1997.
- [54] Y. Sun, D. Wang, P. Sinha, G. M. Carter, and C. R. Menyuk, “Polarization evolution in a 107-km dispersion-managed recirculating loop,” in *Proc. CLEO’00*, (San Francisco, CA), May 2000, paper CML3.
- [55] M. Suzuki, I. Morita, N. Edagawa, S. Yamamoto, H. Taga, and S. Akiba, “Reduction of gordon-haus timing jitter by periodic dispersion compensation in soliton transmission,” *Electron. Lett.*, vol. 31, no. 23, pp. 2027–2029, 1995.
- [56] M. I. Hayee and A. E. Willner, “Pre- and post-compensation of dispersion and nonlinearities in 10-Gb/s WDM systems,” *IEEE Photon. Technol. Lett.*, vol. 9, no. 9, pp. 1271–1273, 1997.
- [57] L. Ding, E. A. Golovchenko, A. N. Pilipetskii, C. R. Menyuk, and P. K. Wai, “Modulated NRZ signal transmission in dispersion maps,” *OSA Trends in Optics and Photonics*, vol. 12, *System Technologies*, A. E. Willner and C. R. Menyuk, eds. Optical Society of American, Washington DC, pp. 204–206, 1997.

- [58] R.-M. Mu and C. R. Menyuk, “Symmetric slope compensation in a long haul WDM system using the CRZ format,” *IEEE Photon. Technol. Lett.* (to be published).
- [59] T. Yu and C. R. Menyuk, “RZ and NRZ signal propagation in optical fiber transmission systems,” in *OSA Annual Meeting*, (Baltimore, MD), Oct. 1998, paper ThQ4.
- [60] R.-M. Mu, T. Yu, V. S. Grigoryan, and C. R. Menyuk, “Dynamics of chirped return-to-zero format,” *J. Lightwave Technol.*, submitted for publication.
- [61] T. Yu, W. M. Reimer, V. S. Grigoryan, and C. R. Menyuk, “A mean field approach to WDM simulations,” *IEEE Photon. Technol. Lett.*, vol. 12, no. 4, pp. 443–445, 2000.
- [62] N. S. Bergano and C. R. Davidson, “Wavelength division multiplexing in long-haul transmission systems,” *J. Lightwave Technol.*, vol. 14, no. 6, pp. 1299–1308, 1996.